HHS Public Access

Author manuscript

Inorg Chem. Author manuscript; available in PMC 2021 July 23.

Published in final edited form as:

Inorg Chem. 2020 December 07; 59(23): 17473–17487. doi:10.1021/acs.inorgchem.0c02722.

Polyazamacrocycle ligands facilitate ^{89}Zr radiochemistry and yield ^{89}Zr complexes with remarkable stability

Darpan N. Pandya[*,a], **Kelly E. Henry**[b], **Cynthia S. Day**[c], **Stephen A. Graves**[a], **Veronica L. Nagle**[b], **Thomas R. Dilling**[b], **Akesh Sinha**[a], **Brandie M. Ehrmann**[d], **Nikunj B. Bhatt**[e], **Yusuf Menda**[a], **Jason S. Lewis**[b,*], **Thaddeus J. Wadas**[a,*]

[a)]Department of Radiology University of Iowa, Iowa City, IA 52242

[b)]Department of Radiology, Memorial Sloan Kettering Cancer Center, New York, NY 10065

[c)]Department of Chemistry, Wake Forest University, Winston-Salem, NC 27109

[d)]Department of Chemistry, University of North Carolina at Chapel Hill, Chapel Hill, NC 27599

[e)]Department of Radiology, Columbia University, New York, NY 10032

Abstract

Over the last three decades, the chemistry of zirconium has facilitated antibody development and the clinical management of disease in the precision medicine era. Scientists have harnessed its reactivity, coordination chemistry and nuclear chemistry to develop antibody-based radiopharmaceuticals incorporating zirconium-89 (^{89}Zr: $t_{½}$ = 78.4 h, β^+: 22.8%, $E_{\beta+max}$ = 901 keV; EC: 77%, E_γ = 909 keV) to improve disease detection, identify patients for individualized therapeutic interventions and monitor their response to those interventions. However, release of the $^{89}Zr^{4+}$ ion from the radiopharmaceutical remains a concern since it may confound the interpretation of clinical imaging data, negatively affect dosimetric calculations and hinder treatment planning. In this report we relate our novel observations involving the use of polyazamacrocycles as zirconium-89 chelators. We describe the synthesis and complete characterization of zirconium 2,2′,2”,2”’-(1,4,7,10-tetraazacyclotridecane-1,4,7,10-tetrayl)tetraacetic acid (Zr-TRITA), zirconium 3,6,9,15-Tetraazabicyclo[9.3.1] pentadeca-1(15),11,13-triene-3,6,9-triacetic acid (Zr-PCTA) and zirconium 2,2’,2”-(1,4,7-triazacyclononane-1,4,7-triyl)triacetic acid (Zr-NOTA). Additionally, we elucidate the solid-state structure of each complex using single crystal x-ray diffraction analysis. Finally, we found that [^{89}Zr]Zr-PCTA and [^{89}Zr]Zr-NOTA demonstrate excellent stability *in vitro* and *in vivo* and provide a rationale for these observations. These innovative findings have the potential to guide the development of safer and more robust immuno-PET agents to improve precision medicine applications.

[*]Corresponding Author Thaddeus J. Wadas, Ph.D., Associate Professor of Radiology, Director, Small Animal Imaging Core, Carver College of Medicine, University of Iowa, 169 Newton Road, Iowa City, IA 52242, phone: (319) 335-5009, fax: (319) 353-6275, thaddeus-wadas@uiowa.edu; Darpan N. Pandya, Ph.D., Associate Research Scientist, Department of Radiology, Carver College of Medicine, University of Iowa, 169 Newton Road, Iowa City, IA 52242, phone: (319) 335-5161, darpan-pandya@uiowa.edu; Jason S. Lewis, Ph.D., Emily Tow Jackson Chair in Oncology, Department of Radiology, Memorial Sloan Kettering Cancer Center, New York, NY 10065, Phone: 646-888-3038, lewisj2@mskcc.org.

Author Contributions

The manuscript was written through contributions of all authors. All authors have given approval to the final version of the manuscript.

Graphical Abstract

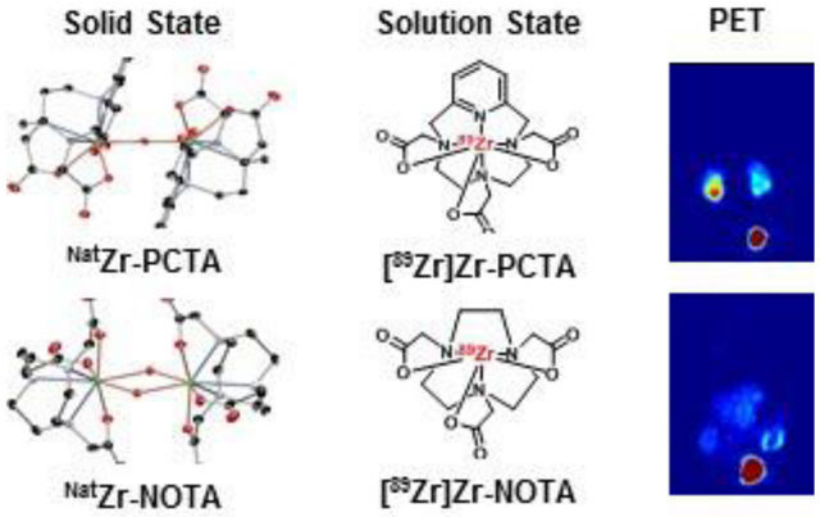

The macrocycles PCTA and NOTA are efficient zirconium-89 chelators. The resulting radiometal complexes can be formed under mild conditions and exhibit remarkable stability *in vitro* and *in vivo*.

Keywords

Polyazamacrocycle; zirconium-89; positron emission tomography; immuno-PET

INTRODUCTION

Zirconium-89 immuno-positron emission tomography (^{89}Zr-immuno-PET), which is the use of ^{89}Zr-radiolabelled monoclonal antibodies (mAbs) in conjunction with current whole-body PET detection, has the potential to enhance the information obtained through traditional biopsy and improve patient care.[1-3] Indeed, important clinical trials are underway to evaluate the utility of ^{89}Zr-immuno-PET for detecting disease, guiding biopsy, stratifying patients for therapy and monitoring therapy response by non-invasively probing receptor expression on tumors of oncology patients.[4,5] For example, Ulaner and colleagues recently sought to determine if ^{89}Zr-trastuzumab PET imaging could be used to detect HER2-positive metastases in patients diagnosed with HER2 negative, primary disease.[6-11] Confirming the authors' hypothesis, ^{89}Zr-trastuzumab PET identified several women who although diagnosed with HER2 negative primary disease had pathologically confirmed HER2 positive distant metastases. However, the authors also observed false-positive findings; several were in osseous metastases. The authors suggested that these findings may result from the $^{89}Zr^{4+}$ ion being released from its chelator and non-specifically localizing in the phosphate rich hydroxylapatite where active bone remodelling is occurring due to metastatic disease. Indeed, several published reports describe the accumulation of radioactivity in bone when ^{89}Zr is chelated to antibodies with desferrioxamine (DFO), which is the only ^{89}Zr chelator currently being used in clinical studies.[12-14] These findings highlight the clinical importance

of developing new ligands that can stably sequester ^{89}Zr during the extended circulation time that these radiopharmaceuticals encounter after patient injection.

Recently, Pandya et al. investigated the use of tetraazamacrocycles as chelators for ^{89}Zr.[15] In this work the authors described the synthesis and characterization of several Zr-cyclen complexes containing carboxylic acid, phosphonate and amide containing pendant arms. These studies revealed all complexes to be octa-coordinate with all four ring nitrogen atoms and pendent arms participating in Zr^{4+} ion coordination. *In vitro* several of the ^{89}Zr-tetraazamacrocycle complexes demonstrated greater resistance to challenge by exogenous ligands, biologically relevant metal ions or serum than [^{89}Zr]Zr-DFO. Biodistribution and small animal PET/CT studies revealed that [^{89}Zr]Zr-DOTA demonstrated extraordinary *in vivo* stability and was far superior to the stability of [^{89}Zr]Zr-DFO. Although extraordinary stability was observed with the former complex, high temperature was required to synthesize it quantitatively, and this was deemed a disadvantage for the synthesis of ^{89}Zr-immuno-PET agents if the DOTA-mAb was going to be radiolabeled with ^{89}Zr directly. Although several two-step radiochemistry procedures published in the literature would alleviate this potential disadvantage,[16-20] it seemed prudent to survey similar ligands to determine if they could be quantitatively radiolabeled with ^{89}Zr at low temperature while providing a stability profile comparable to that of [^{89}Zr]Zr-DOTA. Accordingly, we synthesized Zr-PCTA, Zr-NOTA, Zr-TRITA and Zr-TETA and their ^{89}Zr analogs (Figure 1) to assess how the size and flexibility of the polyazamacrocycle ring influenced the radiochemistry and stability of the resulting radiometal complex *in vitro* and *in vivo*.

RESULTS AND DISCUSSION

Synthesis and Molecular Structure Determination.

Zirconium-89 immuno-PET has enabled significant advances in therapeutic development while its role in the clinical management of disease continues to evolve.[21,22] It has facilitated therapeutic mAb development by reducing the time needed to identify the most promising agents for clinical translation. Further, ^{89}Zr-immuno-PET is expected to become an increasingly powerful clinical tool in the era of personalized medicine since it has the potential to confirm malignancy, elucidate antigen density; optimize pharmacokinetics, provide dosimetry in advance of radioimmunotherapy and describe each lesion's molecular phenotype in a comprehensive manner. However, two important criteria must be satisfied for ^{89}Zr-immuno-PET to be effective. First, the radiopharmaceutical must demonstrate specificity for its biological target. Secondly, once conjugated to the mAb, the ^{89}Zr-chelate complex must remain inert to the biological, chemical and physical forces that will be encountered while circulating within the blood pool over several days. This latter issue may confound the interpretation of clinical imaging data, negatively affect dosimetric calculations and hinder treatment planning. Solving this problem remains an active area of research.[12-14,20,23-40]

Previously, we evaluated tetraazamacrocycles as ^{89}Zr chelators.[15] In that report we evaluated the cyclen–based macrocycles DOTA, DOTP and DOTAM to understand the influence of various pendant arm coordinating units on radiochemistry and stability. Surprisingly, DOTA, a cyclen derivative containing four pendant arms with carboxymethylene coordinating units

yielded a radiometal complex with an *in vitro* and *in vivo* stability that was superior to the other derivatives containing pendant arms with the phosphonate or amide coordinating units. Moreover, [^{89}Zr]Zr-DOTA also demonstrated superior *in vivo* behavior to [^{89}Zr]Zr-DFO, which is currently the radiometal complex being used in clinical ^{89}Zr-immuno-PET applications. This report describes the suitability of the macrocycle ligands TETA, TRITA, PCTA and NOTA as ^{89}Zr chelators; it posits how the size and flexibility of each macrocycle may influence the Zr chemistry of each ligand, the radiochemical synthesis of each radiometal complex, and the *in vitro* and *in vivo* stability of each ^{89}Zr complex.

Following synthetic procedures established for Zr-DOTA,[15] we undertook the synthesis of Zr-TETA (Scheme S1), Zr-TRITA (Scheme S2), Zr-PCTA (Scheme S3) and Zr-NOTA (Scheme S4) using Zr(IV) acetylacetonate ($Zr(AcAc)_4$) as a zirconium source with subsequent synthetic strategies modified from the literature. Unfortunately, Zr-TETA could not be prepared even under forcing conditions using conventional thermal or microwave-assisted strategies; we were unable to characterize this non-radioactive complex further. However, the non-radioactive complexes of Zr-TRITA, Zr-PCTA and Zr-NOTA were successfully prepared in excellent yields and all were fully characterized by HPLC, NMR spectroscopy, and HR-MS analyses (Figures S1-S23). Additionally, each complex yielded single crystals suitable for x-ray diffraction analysis. The complete crystallographic parameters, data collection, refinement information, selected bond lengths, and bond angles of Zr-TRITA, Zr-PCTA and Zr-NOTA are defined in Tables S1-S5, S6-S10, and S11-S15 respectively. The molecular structures of Zr-TRITA, Zr-PCTA and Zr-NOTA are depicted in Figure 2, Figure 3, and Figure 4, respectively. In each case the ligands display a low-symmetry saddle-like conformation. This conformation is characteristic of metal complexes, which demonstrate d^0 electron configurations and lack crystal-field stabilization. While the bond lengths and bond angles of Zr-TRITA, Zr-PCTA and Zr-NOTA are comparable to those observed in structurally characterized Zr complexes,[41-50] each complex demonstrates unique structural features, which have been summarized below.

X-ray diffraction of Zr-TRITA crystals (Figures 2, S24-S30) revealed that the asymmetric unit cell contains three crystallographically-independent molecules, which co-crystallize with three water molecules in the monoclinic Cc space group. The molecular geometry can best be described as a square antiprism. Similar to the Zr-DOTA structure, the Zr^{4+} ion lies closer in proximity to the carboxylate containing pendant arms than to the macrocycle. Analysis of the three crystallographically distinct molecules reveals that the average perpendicular distance from the metal center to the plane described by the four acetate-containing pendant arms of the macrocycle is 1.030 ± 0.002Å while the average perpendicular distance from the metal center to the plane described by the four nitrogen atoms of the macrocycle is 1.280 ± 0.002Å; both distances do not vary significantly from those observed in the Zr-DOTA solid state structure. Interestingly, the introduction of the additional methylene unit into the TRITA backbone increases the *cis*-N-Zr-N bite angle of the cyclam portion of the ligand by 15° when compared to the *cis*-N-Zr-N bite angle exhibited by the cyclen portion of the ligand (85.5(1)° vs. 71.0(1)°). This bite angle is also 13° larger than that observed in the analogous Zr-DOTA complex.[15] The expanded bite angle of the former complex may be a contributing factor to the difficult radiochemistry and poor stability exhibited by [^{89}Zr]Zr-TRITA (*vide infra*).

X-ray diffraction analysis revealed that Zr-PCTA (Figures 3, S31-S34) crystalizes as a binuclear complex in the monoclinic C2/c space group along with four water molecules and its molecular geometry is best described as a distorted square antiprism. The seven coordinate monomers are bridged by one oxygen atom, which lies on the crystallographic 2-fold axis at ½, y, ¼ in the unit cell, to fulfil Zr^{4+} ion's requirement of an octa-coordinate ligand sphere. Interestingly, the pyridyl rings of the PCTA ligands are related by the 2-fold axis and are oriented in a nearly parallel configuration; the angle between them deviates by 7.1°. The perpendicular distance from the metal center to the plane described by the three acetate-containing pendant arms of the macrocycle is 0.9813(4)Å, while the perpendicular distance from the metal center to the plane described by the four nitrogen atoms of the macrocycle is 1.5091(6)Å. This suggests that the Zr^{4+} ion is more closely associated with the pendant arms than the macrocycle. The distances between the Zr^{4+} ions of each monomer subunit and the bridging oxygen atom were observed to be 1.9809(3)Å, while the Zr-O-Zr angle was observed to be 167.32(7)°. These values are similar with published literature describing other Zr-μ-oxo complexes and several observations may explain these results.[51-54] The pyridyl ring of the PCTA ligand most likely increases the rigidity and preorganization of the resulting Zr-PCTA complex. Additionally, numerous inter-and intramolecular hydrogen bonding motifs are observed in the solid state. Both factors probably minimize repulsion energies through enhanced crystal packing and give rise to the shortened bond lengths and pseudo-linear μ-oxo bridge. Finally, the intramolecular distance between the centroids of the pyridyl rings of the PCTA ligands is 6.399Å. The large separation between the rings and their unfavorable orientation about the 2-fold axis disfavors **π-π** stacking, which is a stabilizing phenomenon that has been observed to occur in other transition metal complexes containing similar ligand motifs.[55,56]

X-ray diffraction analysis revealed that Zr-NOTA (Figures 4, S35-S41) also crystalizes as a binuclear complex in the monoclinic $P2_1/n$ space group with six water molecules per dimer. Unlike the other two structures, its geometry is best described as a triangular dodecahedron. The six coordinate monomers, which are defined by the Zr-NOTA subunits are bridged by two OH groups and are related by the crystallographic inversion center at ½, ½, 0 in the unit cell.

The arrangement of the three methylene groups around N3 of the structure demonstrate a slight rotational disorder (93%/7%) around the Zr-N3 bond. The average perpendicular distance from the metal center to the plane described by the three acetate-containing pendant arms of the macrocycle is 0.3820(7) Å, while the perpendicular distance from the metal center to the plane described by the three nitrogen atoms of the macrocycle is 1.8253(5) Å. Similar to the Zr-PCTA structure, this suggests that the Zr^{4+} ion is more closely associated with the pendant arms than the macrocycle. The distances between the Zr^{4+} ions of each monomer subunit and the bridging hydroxide molecules were observed to be unequal with an average distance of 2.1553(7)Å; the Zr-OH-Zr angles were observed to be approximately 111.70(3)°. These observations are consistent with μ-hydroxo and μ-oxo binuclear In^{3+} complexes but dissimilar to binuclear Fe^{3+} complexes reported in the literature.[57,58]

Radiochemical Synthesis.

After completing synthesis and characterization of the reference complexes, we attempted to radiolabel each ligand using [^{89}Zr]Zr(ox)$_2$ and procedures established for preparation of [^{89}Zr]Zr-DFO. However, radiochemical yields were poor (Scheme S5, Table S16). Thus, we used [^{89}Zr]ZrCl$_4$ (Figure S42) as a radioactive precursor and observed that PCTA and NOTA were quantitatively radiolabeled within 60 minutes at 37 °C (Scheme S6, Tables S17, S18, and Figures S43, S46), while TRITA was radiolabeled 80.1 ± 1.2 % within 120 minutes at 99 °C (Table S19, Figure S49). In an attempt to improve the reaction kinetics, a microwave-assisted synthesis using forcing conditions was required to quantitatively prepare [^{89}Zr]Zr-TRITA (Table S20, Figure S50). Despite repeated attempts to prepare [^{89}Zr]Zr-TETA using conventional and microwave-assisted strategies, radiochemical yields were poor even under the most forceful conditions (Table S21, Figure S53). The radiochemical yield and purity of [^{89}Zr]Zr-PCTA, [^{89}Zr]Zr-NOTA, and [^{89}Zr]Zr-TRITA were confirmed by radio-TLC (Figures S44, S47, and S51) and radio-HPLC (Figures S45, S48, and S52). Optimized radiochemical synthesis conditions are presented in Table 1. The molar activity (A_m) for each radiometal complex is in good agreement with the A_m of other ^{89}Zr complexes reported in the literature.[15] Based upon our attempts to prepare [^{89}Zr]Zr-TETA, [^{89}Zr]Zr-TRITA and our previous work with [^{89}Zr]Zr-DOTA, the ease of radiochemical synthesis can be described as [^{89}Zr]Zr-DOTA > [^{89}Zr]Zr-TRITA >>> [^{89}Zr]Zr-TETA. While increasing the cavity size would have been thought to facilitate ^{89}Zr radiochemistry, perhaps the introduction of additional methylene units increases the cavity size and decreases the molecular orbital overlap between the bonding orbitals of the $^{89}Zr^{4+}$ ion and the bonding orbitals of the macrocycles TRITA and TETA. Although we were unable to determine the molecular structure of Zr-TETA, we were fortunate enough to elucidate the crystal structures of Zr-TRITA and Zr-DOTA. In these structures we did observe that the *cis*-N-Zr-N bite angles were different and may be enough to disrupt the molecular orbital interactions necessary for metal-ligand bonding. Similar observations were reported to influence the preparation and stability of Ln^{3+} tetraazamacrocycle complexes. For example, ease of synthesis and kinetic inertness of Ln^{3+} tetraazamacrocycle complexes decreased by several orders of magnitude when considering the reactivity of the 12-membered DOTA, 13-membered TRITA and then the 14 membered TETA macrocycles.[59,60] Additionally, the degree of preorganization of each ligand may also influence the radiochemistry.[59,61-63] The non-complexed $DOTA^{4-}$ crystal structure reveals that the four carboxymethyl pendant arms are in the *syn* configuration with respect to the macrocycle plane. On complexation with $^{89}Zr^{4+}$ ion, the ligand would have to undergo minimal reorganization to accommodate the radioactive ion. Contrarily, the $TETA^{4-}$ structure reveals that the adjacent carboxymethyl pendant arms are in an *anti*-configuration with respect to the macrocycle plane. As a result, significant ligand rearrangement would be required to achieve the *syn* configuration necessary to form the [^{89}Zr]Zr-TETA complex. While the crystal structure of $TRITA^{4-}$ is not available, it is conceivable that this ligand has at least one carboxymethylene containing pendant arm in the *anti* configuration, and this may explain why forcing conditions are necessary to prepare [^{89}Zr]Zr-TRITA. Furthemore, additional literature suggests that enthalpic effects that arise from the inability of larger macrocycles to effectively chelate large metal ions also plays a role in the lack of complex formation and instability.[64]

Lipophilicity (LogP) Determination.

Lipophilicity (LogP) represents a fundamental physiochemical property that influences the adsorption, distribution, metabolism and elimination of ^{89}Zr-complexes *in vivo*.[65] Based upon the water/octanol partition method all complexes demonstrate hydrophilic character, which is attributed to the numerous hydrogen bonds these complexes experience in solution and is supported by the multiple water molecules engaged in hydrogen bonding with each Zr complex as revealed by single crystal analysis. All values (Table S22) suggest that renal excretion would be a preferred route of elimination after *in vivo* injection. Interestingly, [^{89}Zr]Zr-NOTA has a LogP value (−2.51 ± 0.01) that is more positive than the LogP value of [^{89}Zr]Zr-DFO (−2.83 ± 0.03).[15] Despite the pyridyl ring of the PCTA macrocycle, its LogP value (−3.09 ± 0.03) was more negative than the LogP of [^{89}Zr]Zr-DFO and similar to that of [^{89}Zr]Zr-TRITA (−3.13 ± 0.02). However, all were more positive than the LogP value reported for [^{89}Zr]Zr-DOTA (−3.80 ± 0.04).[15]

In Vitro Stability Studies.

Similar to our previous work evaluating ^{89}Zr-tetraazamacrocycles,[15] the *in vitro* stability of [^{89}Zr]Zr-NOTA, [^{89}Zr]Zr-TRITA and [^{89}Zr]Zr-PCTA were evaluated by challenging them with excess EDTA, high concentrations of biologically relevant metal ions, or human serum proteins. Over seven days, these experiments revealed that [^{89}Zr]Zr-PCTA was inert to transchelation by a 1000-fold excess of EDTA at pH 5 or pH 7. After seven days in the presence of a 1000-fold excess of EDTA at pH 5, approximately 35% of the activity initially associated with [^{89}Zr]Zr-NOTA was transchelated by EDTA, while approximately 90% of the initial activity associated with the TRITA ligand was transchelated to EDTA under the same conditions. Based upon our EDTA challenge studies, the order of ^{89}Zr complex stability can be described as [^{89}Zr]Zr-PCTA > [^{89}Zr]Zr-NOTA >> [^{89}Zr]Zr-TRITA (Table 2).

Polyazamacrocycles can chelate numerous, biologically relevant metal ions potentially creating a second mechanism for $^{89}Zr^{4+}$ ion dissociation from its chelator *in vivo*.[25] To assess the ability of the ^{89}Zr complexes to resist demetallation, we mixed each radiometal complex with an excess concentration of metal salts in aqueous buffer. No demetallation of [^{89}Zr]Zr-PCTA was observed over the 7-day experiment (Table 3). In contrast, [^{89}Zr]Zr-NOTA remained only 88% and 90% intact when challenged with Cu^{2+} ions or Ga^{3+} ions, respectively during the same study period. Finally, [^{89}Zr]Zr-TRITA remained only 60% and 62% intact when challenged with Cu^{2+} ions or Ga^{3+} ions, respectively by the end of the study. The overall order of ^{89}Zr complex stability mirrored our results in the EDTA challenge experiments.

Incubation in human serum (Figures S54, S55, Table 4) revealed [^{89}Zr]Zr-PCTA was the most resistant to serum protein challenge, while [^{89}Zr]Zr-NOTA was slightly less inert. After three days, 96% of the original activity remained chelated to the latter polyazamacrocycle. Finally, only 80% and 32% of the original radioactivity associated with the TRITA macrocycle remained chelated to it after one and seven days, respectively making [^{89}Zr]Zr-TRITA the most vulnerable to transchelation by serum proteins.

Biodistribution Studies in Mice.

We then evaluated the *in vivo* behavior of [^{89}Zr]Zr-TRITA, [^{89}Zr]Zr-PCTA or [^{89}Zr]Zr-NOTA in acute biodistribution studies involving normal mice. Results are shown in Tables S23-S25 and Figures 5, S56-S58. At 2 h post-injection (p.i.), animals injected with [^{89}Zr]Zr-TRITA demonstrated elevated levels of blood-associated radioactivity and these levels remained elevated at all time points of the study. Conversely, [^{89}Zr]Zr-PCTA and [^{89}Zr]Zr-NOTA were cleared from the blood pool much more efficiently and by 72 h p.i., the amount of radioactivity associated in the blood of animals receiving [^{89}Zr]Zr-TRITA was still significantly greater than observed for those animals receiving either [^{89}Zr]Zr-PCTA or [^{89}Zr]Zr-NOTA ([^{89}Zr]Zr-TRITA vs. [^{89}Zr]Zr-PCTA vs. [^{89}Zr]Zr-NOTA [blood (72 h p.i., %ID/g ± SD); one-way ANOVA]: 0.004 ± 0.008 vs. 0.000 ± 0.001 vs. 0.001 ± 0.0002; [$F(2,13) = 29.37$, $p < 0.0001$]. At 72 h p.i., animals injected with [^{89}Zr]Zr-TRITA also had 10- and 5-fold more radioactivity associated with liver tissue when compared to animals receiving either [^{89}Zr]Zr-PCTA or [^{89}Zr]Zr-NOTA, respectively ([^{89}Zr]Zr-TRITA vs. [^{89}Zr]Zr-PCTA vs. [^{89}Zr]Zr-NOTA [liver (72 h p.i., %ID/g ± SD); one-way ANOVA]: 0.304 ± 0.022 vs. 0.030 ± 0.003 vs. 0.069 ± 0.007; [$F(2,15) = 731$, $p < 0.0001$]. A similar trend was observed when comparing radioactivity associated with kidney tissues. Animals receiving [^{89}Zr]Zr-TRITA retained the most radioactivity in the kidney with only 54% of the 2 h activity being excreted at 72 h p.i. In contrast, 79% and 71% of the 2 h activity in the kidney tissue of animals receiving either [^{89}Zr]Zr-PCTA or [^{89}Zr]Zr-NOTA had been excreted at the same time point ([^{89}Zr]Zr-TRITA vs. [^{89}Zr]Zr-PCTA vs. [^{89}Zr]Zr-NOTA [kidney (72 h p.i. %ID/g ± SD); one-way ANOVA]: 0.59 ± 0.04 vs. 0.15 ± 0.01 vs. 0.30 ± 0.02; [$F(2,15) = 460$, $p < 0.0001$]. Finally, radioactivity in the bone tissue of animals receiving [^{89}Zr]Zr-TRITA was elevated (2.06 ± 0.5 %ID/g) at 2 h p.i. and increased by nearly 400% at the conclusion of the study. In contrast radioactivity levels in the bones of animals receiving either [^{89}Zr]Zr-PCTA or [^{89}Zr]Zr-NOTA were observed to be much lower at 2 h p.i. and further decreased by 10% and 50%, respectively by 72 h p.i. ([^{89}Zr]Zr-TRITA vs. [^{89}Zr]Zr-PCTA vs. [^{89}Zr]Zr-NOTA [bone (72 h p.i., %ID/g ± SD); one-way ANOVA]: 8.04 ± 1.5 vs. 0.094 ± 0.006 vs. 0.046 ± 0.006; [$F(2,15) = 176$, $p < 0.0001$].

Small Animal PET Imaging Studies.

Although [^{89}Zr]Zr-TRITA was not considered further due to its extremely poor biodistribution profile, [^{89}Zr]Zr-PCTA and [^{89}Zr]Zr-NOTA were evaluated in normal mice using small animal PET (Figures 6, S59). Analysis of the dynamic PET data revealed that [^{89}Zr]Zr-PCTA and [^{89}Zr]Zr-NOTA underwent rapid perfusion and clearance from the blood pool and liver tissue during the first 60 minutes of the study. Both radiometal complexes also exhibited renal excretion. However, the time activity curves were dissimilar with [^{89}Zr]Zr-NOTA exhibiting-more efficient renal clearance. The dissimilar urine excretion profiles may be caused by the normal intra-variability that can be associated within individual mice.[66,67] Another explanation may be that the ligand associated with the radiometal complex influences this physiological parameter. A similar phenomenon was observed when the renal clearance of [^{68}Ga]Ga-PCTA and [^{68}Ga]Ga-NOTA derivatives were evaluated in normal mice with the [^{68}Ga]Ga-NOTA derivatives being excreted more efficiently over time.[68] Interestingly, renal and hepatobiliary excretion of both radiometal complexes were observed as the experimental time course progressed from 1 h p.i. to 24 h p.i. While the cause is

uncertain, a similar bimodal excretion pattern was observed when [^{89}Zr]Zr-LI-1,2-HOPO was evaluated in acute biodistribution and small animal PET/CT studies.[31]

Dosimetric Calculations.

Based upon these results and our previously published data describing [^{89}Zr]Zr-DOTA and [^{89}Zr]Zr-DFO, we calculated the dosimetric profiles in tissues for each ^{89}Zr-complex. While we acknowledge that the dosimetric profiles of the radiometal complexes will be completely different from the calculated tissue dosimetry obtained using a radiolabeled mAb, we thought it prudent to evaluate this criterion since dissociation of the radiometal or intact radiometal complex from the circulating mAb may influence the radiation absorbed by critical tissues such as the liver, kidney and bone marrow. Except for [^{89}Zr]Zr-TRITA, all complexes cleared from the whole body at exceptionally fast rates; less than 1% of the administered activity remained in the body at 24 hours post-injection. Dosimetry results (Table 5) demonstrate minimal variability in whole animal mean doses, ranging from 2.3 – 2.7 mGy/MBq. Conversely, [^{89}Zr]Zr-TRITA demonstrated a mean total body dose of 65 mGy/MBq. The 25-fold higher total body mean dose and 85-fold higher dose to bone with [^{89}Zr]Zr-TRITA can be attributed to the substantial accumulation of radioactivity in the bones, increasing from 7% IA at 2 h p.i. to 16% IA at 48 h p.i. Although only estimates from a sub-sample of each mouse skeleton, it is clear that complex instability leads to significantly increased bone accumulation, and associated whole body dose per administered activity. Among other complexes, dosimetric differences were minimal.

Retrospective Analysis.

Similar to our previous work, we attempted to place our results in context by comparing them with published studies that describe the *in vitro* and *in vivo* behavior of other ^{89}Zr chelators, (Tables S26-S28).[15] Variability in study design or unreported data prevented direct comparisons among all ligands, but comparisons were made when possible. Furthermore, we have excluded [^{89}Zr]Zr-TRITA from this comparison due to its exceedingly poor performance *in vitro* and *in vivo*.

In vitro data suggest that when challenged with 1000-fold excess EDTA (pH 7) for seven days, [^{89}Zr]Zr-PCTA was as resistant to transchelation as several [^{89}Zr]Zr-TAM and [^{89}Zr]Zr-HOPO complexes.[34,38] [^{89}Zr]Zr-NOTA was less resistant to transchelation being only 71% intact under the same conditions. Metal ion competition studies revealed that [^{89}Zr]Zr-PCTA and [^{89}Zr]Zr-NOTA were as resistant to transmetallation as [^{89}Zr]Zr-DOTA when exposed to Fe^{3+} ions.[15] [^{89}Zr]Zr-PCTA also demonstrated similar resistance to transmetallation as [^{89}Zr]Zr-HOPO and [^{89}Zr]Zr-DOTA when challenged with Zn^{2+}, Co^{2+}, Mg^{2+}, Gd^{3+}, Cu^{2+} and Ga^{3+} ions.[15] However, [^{89}Zr]Zr-NOTA was more susceptible to transmetallation when challenged with Cu^{2+} and Ga^{3+} ions.[15] This latter result is not surprising since NOTA and its analogs have gained popularity in the radiopharmaceutical community as useful chelators for $^{64}Cu^{2+}$ and $^{68}Ga^{3+}$ ions.[14,25,69,70] Acute biodistribution studies revealed that [^{89}Zr]Zr-PCTA and [^{89}Zr]Zr-NOTA demonstrated *in vivo* behavior that was comparable to [^{89}Zr]Zr-LI-1,2-HOPO.[31]

However, both displayed better *in vivo* behavior than several ligands containing terephthalamide, 3-hydroxypyridin-2-one or hydroxyisophthalamide coordinating units.[29,34,38] For example, [^{89}Zr]Zr-PCTA retained 22-and 110-fold less activity in liver and kidney tissue, respectively when compared to [^{89}Zr]Zr-TAM-2.[34] Similarly, [^{89}Zr]Zr-NOTA retained 8-and 99-fold less activity in the same tissues after 24 h.[34] Finally, while neither [^{89}Zr]Zr-PCTA nor [^{89}Zr]Zr-NOTA demonstrated *in vivo* behavior that was superior to [^{89}Zr]Zr-DOTA, their *in vivo* behavior was similar or superior to [^{89}Zr]Zr-DFO and makes them worthy of further study (Figure S56-S58).[15]

The data presented here augments what is known about the ^{89}Zr radiochemistry of polyazamacrocycles and reveal that PCTA and NOTA should be considered along with DOTA as promising ^{89}Zr chelators. However, we acknowledge that their utility will only be recognized if they can be incorporated into a clinically relevant chelator-mAb conjugate, the conjugate can be radiolabeled with ^{89}Zr in high specific activity and the resulting ^{89}Zr-immuno-PET agent can resist the biological, chemical and physical forces that will be encountered in the systemic circulation over several days. These studies are currently underway in our laboratory.

CONCLUSION

Utilizing the reactivity, coordination chemistry and nuclear chemistry of zirconium we describe the preparation and characterization of Zr-TETA, Zr-TRITA, Zr-PCTA and Zr-NOTA complexes. Similar to Ln^{3+} tetraazamacrocycles complexes, complexes containing macrocycles that were smaller and more preorganized could be prepared under milder conditions. Additionally, the solid-state structures of the Zr complexes derived from the TRITA, PCTA and NOTA ligands further reinforce the idea that the Zr^{4+} ion prefers an octa-coordinate ligand environment and will form binuclear complexes to saturate its ligand sphere when the monomeric ligand is incapable of providing eight coordinating units. The ^{89}Zr radiochemistry paralleled our non-radioactive synthesis results. The preparation of [^{89}Zr]Zr-TETA could not be accomplished while the preparation of [^{89}Zr]Zr-TRITA could be achieved only under forcing conditions. Conversely, the quantitative radiolabeling of PCTA and NOTA with ^{89}Zr occurred under mild conditions. Additionally, while [^{89}Zr]Zr-TRITA demonstrated poor stability, [^{89}Zr]Zr-PCTA and [^{89}Zr]Zr-NOTA demonstrated robust *in vitro* stability and *in vivo* behavior. Our novel observations demonstrate that polyazamacrocycles are efficient ^{89}Zr chelators. Considering polyazamacrocycles can chelate a variety of radioisotopes for imaging and therapy their use in immuno-PET applications may create new strategies for theranostic development and improve precision medicine applications.

MATERIALS AND METHODS

Abbreviations

DFO: Deferoxamine; PCTA: 3,6,9,15-Tetraazabicyclo[9.3.1]pentadeca-1(15),11,13-triene-3,6,9-triacetic acid; NOTA: 2,2’,2”-(1,4,7-triazacyclononane-1,4,7-triyl)triacetic acid; TRITA: 2,2’,2”,2”’-(1,4,7,10-tetraazacyclo tridecane-1,4,7,10-tetrayl)tetraacetic acid; TETA: 2,2’,2”,2”’-(1,4,8,11-tetraazacyclotetradecane-1,4,8,11-tetrayl)tetraacetic acid;

EDTA: Ethylenediaminetetraacetic acid; $Zr(AcAc)_4$: Zirconium(IV) acetylacetonate; $Zr(ox)_2$: Zirconium(IV) Oxalate; TFA: Trifluoroacetic acid; MeOH: Methanol; NH_4Cl: Ammonium chloride; NH_4OAc: Ammonium acetate; NaOAc: Sodium acetate; TMAA: Tetramethylammonium acetate; MES: 2-(N-morpholino)ethanesulfonic acid; HEPES: 4-(2-Hydroxyethyl) piperazine-1-ethanesulfonic acid; TRIS: Tris(hydroxymethyl)aminomethane; NMR: Nuclear Magnetic Resonance; HMBC: Heteroatom Multiple-Bond Correlation; HMQC: Heteronuclear Multiple Quantum Coherence; UV-HPLC: Ultra-Violate High performance liquid chromatography; RT: Retention Time; R_f: Retention Factor; ESI-HR-MS: Electrospray Ionization High Resolution Mass Spectrometry; HS: Human Serum; ITLC: Instant Thin Layer Chromatography; kBq: Kilobecquerel; MBq: Megabecquerel; %ID/g: Percent Injected Dose Per Gram; P.I.: Post-injection; ROI: Region of Interest; CPM: Counts per Minute; TLC: Thin Layer Chromatography; PET: Positron Emission Tomography; CT: Computed Tomography

Experimental Methods

Zirconium-89 (^{89}Zr: ($t_{½}$ = 78.4 h, β^+: 22.8 %, $E_{\beta+max}$ = 901 keV; EC: 77%, E_γ = 909 keV) was purchased from Sophie, Inc. (Dulles, VA). Unless otherwise noted, all other chemicals were purchased from Sigma-Aldrich Chemical Co. (St. Louis, MO, USA), and solutions were prepared using ultrapure water (18 MΩ-cm resistivity). Macrocyclic ligands (PCTA, NOTA, TRITA and TETA) were purchased from CheMatech, Inc. (Dijon, France). High-resolution mass spectrometry data was acquired using a Thermo LTQ-FT (7 Tesla) system at the University of North Carolina Chapel Hill Mass Spectrometry Core Laboratory. NMR spectra were obtained using a Bruker DRX 500 MHz spectrometer equipped with a 5mm tbi z-axis gradient probe. All data were collected and processed with Topspin 1.3 using standard Bruker processing parameters. 2D ^1H-^1H gsCOSY, gsHMQC and gsHMBC were collected as 2K by 256 point data sets at 25 °C and processed to 1K x 512 blocks. ^1H (500 MHz) chemical shifts are reported in parts per million (ppm) relative to the solvent resonances, taken as δ 4.79 for D_2O. Solvent suppression (1D ^1H NMR) was carried out with pre-saturation of the HOD signal. ^{13}C NMR (126 MHz) chemical shifts were referenced externally to TSP (0.00 ppm). The NMR spectra of Zr-TRITA complex were obtained at 80 °C.

Single crystal x-ray crystallography analysis of Zr-TRITA, Zr-PCTA and Zr-NOTA was performed on a Bruker APEX CCD system equipped with a graphite monochromator and a Mo Kα sealed x-ray tube (λ = 0.71073 Å). X-rays were provided by a fine-focus sealed x-ray tube operated at 50kV and 30mA. Data was refined using commercially available software packages. the following software packages.[71-76] Additional details specific to each complex can be found in the supporting information.

Radiochemistry reaction progress and purity were analyzed by using an analytical HPLC system (Waters, Milford, MA), which runs Empower software and is configured with a 1525 binary pump, 2707 autosampler, 2998 photodiode array detector, 2475 multichannel fluorescence detector, 1500 column heater, fraction collector, HYPERCARB C18 column (5 μ, 4.6 × 100 mm, Thermo Scientific) and a Carrol Ramsey 105-s radioactivity detector (Berkeley, CA). All ligands (PCTA, NOTA, TRITA and TETA) and associated ^{Nat}Zr-

complexes were monitored at 201 nm using a mobile phase consisting of 0.1% TFA/H_2O (solvent A) and 0.1% TFA/acetonitrile (solvent B), and a gradient consisting of 0% B to 70% B in 20 min at a flow rate of 1 mL/min. In addition, radio-TLC was conducted on a Bioscan AR 2000 radio-TLC scanner equipped with a 10% methane : argon gas supply and a PC interface running Winscan v.3 analysis software (Eckert & Ziegler, Berlin, DE). Microwave heating was performed using Biotage® Initiator (Biotage AB, Uppsala, Sweden) microwave synthesizer. Varian ITLC-SA strips (Agilent Technologies, Santa Clara, CA) and Merck C-18 TLC plates were employed using a 50 mM M EDTA (pH 5) and 1:1 MeOH:10% NH_4Cl solution as eluents respectively, and ^{89}Zr-Oxalate or $^{89}ZrCl_4$ as a standard control. Radioactive samples were counted using either a CRC-25R radioisotope calibrator (Capintec, Inc.) or a Perkin Elmer 2480 Wizard® gamma counter (Waltham, MA) with an energy window of 500-1500 keV. A microPET Focus 120 scanner (Concorde Microsystems, Knoxville, Tennessee) was used to obtain static scans at the desired time points with at least 10 million coincident events and ASIPro VM software was used to analyze acquired images.

For statistical analysis, all plots were generated using GraphPad Prism 5.0 software (San Diego, CA). Student's t tests (two-tailed, unpaired) or one-way analysis of variance (ANOVA) with Tukey's multiple comparison post-test were performed. $p<0.05$ was considered statistically significant. Within the text, Student's t test data is presented as mean ± SD or mean (95% confidence intervals), while Anova data is presented as $\boldsymbol{F}$(degrees of freedom between groups (k-1), degrees of freedom within groups (N-k)) = F ratio, p value).

Attempted Synthesis of Zr-TETA.

ZrAcAc (54 mg, 0.111 mmol) was added to a solution of TETA (40 mg, 0.092 mmol) in 20 mL of methanol. The resulting solution was refluxed for 3 h. No product formation was observed.

Synthesis of Zr-TRITA.

ZrAcAc (390 mg, 0.80 mmol) was added to a solution of TRITA (280 mg, 0.67 mmol) in 40 mL of methanol. The resulting solution was refluxed for 2 h. As the reaction proceeded, a white precipitate formed. It was filtered, washed with MeOH (3 X 10 mL), and dried in an oven (304 mg, 90% yield). Formation was confirmed by HPLC (Fig. S1), NMR spectroscopy (Figs. S2-S6), and HRMS analysis (Fig. S7). ^{1}H NMR (400 MHz, D_2O): δ 4.56 – 3.98 (m, 6H), 3.92 – 3.58 (m, 12H), 3.55 – 3.36 (m, 6H), 2.49 – 2.45 (m, 2H); ^{13}C NMR (101 MHz, D_2O) Major and Minor: δ 21.75, 52.06, 53.14, 53.32, 53.84, 54.63, 56.34, 57.30, 57.70, 58.39, 58.83, 60.75, 60.96, 62.89, 63.39, 65.65, 66.70, 68.30, 68.62, 72.77, 177.70, 178.81, 179.17, 179.45; HRMS (ESI FT-ICR): Calculated for $C_{17}H_{27}N_4O_8Zr$, 505.0860 [$(M+H)^+$] Found: 505.0853 [$(M+H)^+$]. Crystals suitable for X-ray structure determination were grown by dissolving Zr-TRITA in water at 100 °C and allowing the solvent to slowly evaporate at room temperature.

Synthesis of Zr-PCTA.

ZrAcAc (400 mg, 0.82 mmol) was added to a solution of PCTA (259 mg, 0.68 mmol) in 30 mL of methanol. The resulting solution was refluxed for 2 h. As the reaction proceeded, a

white precipitate formed. It was filtered, washed with MeOH (3 X 10 mL), and dried in an oven (294 mg, 92% yield). Formation was confirmed by HPLC (Fig. S8), NMR spectroscopy (Figs. S9-S13), and HRMS analysis (Fig. S14). ^{1}H NMR (400 MHz, D_2O) Major: δ 8.09 – 8.02 (m, 1H), 7.51 (d, J = 7.8 Hz, 1H), 4.74 (d, J = 17.1 Hz, 2H), 4.47 (d, J = 17.1 Hz, 1H), 4.05 (d, J = 16.9 Hz, 1H), 3.77 (d, J = 9.0 Hz, 1H), 3.63 (s, 1H), 3.08 – 2.84 (m, 2H), 2.70 – 2.52 (m, 2H). Minor: δ 8.17 – 8.10 (m, 1H), 7.58 (d, J = 7.9 Hz, 1H), 4.57 (d, J = 16.3 Hz, 1H), 4.30 (d, J = 16.4 Hz, 1H), 3.80 (d, J = 7.7 Hz, 1H), 3.50 (d, J = 16.9 Hz, 1H), 3.63 (s, 1H), 3.19 (m, 2H), 2.84 – 2.74 (m, 1H), 2.42 (m, 1H); ^{13}C NMR (101 MHz, D_2O) Major and Minor: δ 57.45, 58.00, 58.20, 59.03, 63.70, 63.95, 65.30, 66.05, 122.12, 122.78, 142.90, 143.74, 158.15, 158.21, 178.60, 179.14, 179.61, 179.79·; HRMS (ESI FT-ICR): Calculated for $C_{17}H_{21}N_4O_6Zr$, 467.0499 [$(M)^+$] Found: 467.0490 [$(M)^+$]. Crystals suitable for X-ray structure determination were grown by dissolving Zr-PCTA in water at 80 °C and allowing the solvent to slowly evaporate at room temperature.

Synthesis of Zr-NOTA.

ZrAcAc (619 mg, 1.27 mmol) was added to a solution of NOTA (321 mg, 1.06 mmol) in 30 mL of methanol. The resulting solution was refluxed for 2 h. As the reaction proceeded, a white precipitate formed. It was filtered, washed with MeOH (3 X 10 mL), and dried in an oven (493 mg, 95% yield). Formation of Zr-NOTA-AcAc complex was confirmed by HPLC (Fig. S15), NMR spectroscopy (Figs. S16-S22), and HRMS analysis (Fig. S23). ^{1}H NMR (400 MHz, D_2O): δ 5.95 (s, 1H), 3.99 (s, 2H), 3.87 – 3.60 (m, 6H), 3.50 – 3.11 (m, 10H), 2.13 (s, 3H), 2.05 (s, 3H); ^{13}C NMR (101 MHz, D_2O) δ 24.53, 27.19, 55.50, 56.54, 57.08, 65.84, 66.60, 105.96, 177.76, 178.62, 184.85, 197.38, (minor spices 24.58, 27.24, 30.46, 179.13, 184.90, 197.43); HRMS (ESI FT-ICR): Calculated for $C_{17}H_{26}N_3O_8Zr$, 490.0761 [$(M+AcAc+H)^+$] Found: 490.0767 [$(M+AcAc+H)^+$]. Crystals suitable for X-ray structure determination were grown by dissolving Zr-NOTA-AcAc in water at 90 °C and allowing the solvent to slowly evaporate at room temperature.

Radiolabeling of Polyazamacrocyclic Ligands (PCTA, NOTA, TRITA, and TETA) with [^{89}Zr]Zr(ox)$_2$.

The complexation of ^{89}Zr with tetraazamacrocyclic ligands (PCTA, NOTA, TRITA, and TETA) was achieved by reacting 10-50 μg (1-5 μL, 10 mg/mL in water) of each ligand with an aliquot of [^{89}Zr]Zr(ox)$_2$ (0.4-0.5 mCi, 16.5-20.5 MBq) diluted in 100 μL of water and pH adjusted to 6.9-7.3 using 1 M Na_2CO_3 or 0.5 M HEPES (pH 7.1-7.3). Reactions were incubated at 99ºC for 2 h in a thermomixer (700 rpm). Formation of [^{89}Zr]Zr-PCTA, [^{89}Zr]Zr-NOTA, [^{89}Zr]Zr-TRITA and [^{89}Zr]Zr-TETA complexes was monitored by radio-TLC using Varian ITLC-SA strips and 50 mM EDTA (pH 5) as the mobile phase.

Preparation of [^{89}Zr]Zr-chloride.

[^{89}Zr]$ZrCl_4$ was produced using a procedure modified from the literature.[24] Briefly, a [^{89}Zr]Zr-oxalate solution in 1.0 M oxalic acid was loaded onto an activated Waters Sep-pak Light accell plus QMA strong anion exchange cartridge (300 Å pore size, 37–55 μm particle size, 230 μeq/gram ion exchange capacity), pre-washed with 6 ml MeCN, 10 ml 0.9% saline and 10 ml water. The cartridge was then washed with water (>50 ml) to remove oxalic acid

and the activity eluted with 100% recovery of ^{89}Zr by chloride ion exchange with 400–500 μl of 1.0 M HCl(aq.).

Radiochemical Synthesis of [^{89}Zr]Zr-PCTA with [^{89}Zr]ZrCl$_4$:

Complexing ^{89}Zr with the tetraazamacrocyclic ligand PCTA was achieved by reacting 15-20 μg (15-20 μL, 1.0 mg/mL in water) of ligand PCTA with an aliquot of [^{89}Zr]ZrCl$_4$ (1.1-1.5 mCi, 41.6-55.5 MBq) diluted in 200 μL of 0.5 M HEPES (pH 7.2) followed by 60 min incubation at 37 ºC in a thermomixer (550 rpm). The results of radiochemistry studies with different reaction buffers, time, and temperature are summarized in Table S17. Formation of [^{89}Zr]Zr-PCTA complex was monitored by radio-TLC using a mobile phase consisting of 50 mM EDTA (pH 5) on Varian ITLC-SA strips. In this ITLC-SA system, free ^{89}Zr formed a complex with EDTA and eluted with the solvent front (R_f ~ 1), while [^{89}Zr]Zr-PCTA complex remained at the origin (R_f ~ 0) (Figs. S43, S44). The identity of the radioactive complex [^{89}Zr]Zr-PCTA was further confirmed by comparing its radio-HPLC elution profile to the UV-HPLC spectrum of nonradioactive ^{Nat}Zr-PCTA (Fig. S45).

Radiochemical Synthesis of [^{89}Zr]Zr-NOTA with [^{89}Zr]ZrCl$_4$:

Complexing ^{89}Zr with the triazamacrocyclic lig- and NOTA was achieved by reacting 15-17 μg (15-17 μL, 1.0 mg/mL in water) of ligand NOTA with an aliquot of [^{89}Zr]ZrCl$_4$ (1.1-1.5 mCi, 41.7-55.7 MBq) diluted in 200 μL of 0.5 M HEPES (pH 7.2) followed by 60 min incubation at 37 ºC in a thermomixer (550 rpm). The results of radiochemistry studies with different reaction buffers, time, and temperature are summarized in Table S18. Formation of [^{89}Zr]Zr-NOTA complex was monitored by radio-TLC using a mobile phase consisting of 50 mM EDTA (pH 5) on Varian ITLC-SA strips. In this ITLC-SA system, free ^{89}Zr formed a complex with EDTA and eluted with the solvent front (R_f ~ 1), while [^{89}Zr]Zr-NOTA complex remained at the origin (R_f ~ 0) (Figs. S46, S47). The identity of the radioactive complex [^{89}Zr]Zr-NOTA was further confirmed by comparing its radio-HPLC elution profile to the UV-HPLC spectrum of nonradioactive ^{Nat}Zr-NOTA (Fig. S48).

Radiochemical Synthesis of [^{89}Zr]Zr-TRITA with [^{89}Zr]ZrCl$_4$ (Conventional Heating Strategy):

Complexing ^{89}Zr with the tetraazamacrocyclic ligand TRITA was achieved by reacting 10-15 μg (30-35 μL, 1.0 mg/mL in water) of ligand TRITA with an aliquot of [^{89}Zr]ZrCl$_4$ (0.46-0.49 mCi, 17.1-18.1 MBq) diluted in 200 μL of 0.5 M HEPES (pH 7.2) followed by 120 min incubation at 99 ºC in a thermomixer (550 rpm). The results of radiochemistry studies with different buffers are summarized in Table S19. Formation of [^{89}Zr]Zr-TRITA complex was monitored by radio-TLC using a mobile phase consisting of 50 mM EDTA (pH 5) on Varian ITLC-SA strips. In this ITLC-SA system, free ^{89}Zr formed a complex with EDTA and eluted with the solvent front (R_f ~ 1), while [^{89}Zr]Zr-TRITA complex moved from origin (R_f = 0.20-0.25) (Fig. S49).

(Microwave Assisted Synthesis):

Complexing ^{89}Zr with the tetraazamacrocyclic ligand TRITA was achieved by reacting 18-24 μg (18-24 μL, 1.0 mg/mL in water) of ligand TRITA with an aliquot of [^{89}Zr]ZrCl$_4$

(1.1-1.4 mCi, 40.7-51.8 MBq) diluted in 250 μL of water and pH adjusted to 3.9-4.2 using 0.5 M HEPES (50-70 μL, pH 7.1 -7.3). The sealed vial containing the reaction mixture was placed in the microwave reactor, stirred for 2 min, and then heated at 180 ºC for 20 min. The results of radiochemistry studies with different reaction pH and temperature are summarized in Table S20. Formation of [^{89}Zr]Zr-TRITA complex was monitored by radio-TLC using a mobile phase consisting of 1:1 MeOH: 10% NH_4Cl on C-18 plates and 50 mM EDTA (pH 5) on Varian ITLC-SA strips. In the C-18 system, un-chelated ^{89}Zr remained at the origin (R_f ~ 0), while [^{89}Zr]Zr-TRITA complex moved near the solvent front (R_f = 0.85-0.90). In the ITLC-SA system, free ^{89}Zr formed a complex with EDTA and eluted with the solvent front (R_f ~ 1), while [^{89}Zr]Zr-TRITA complex moved from origin (R_f = 0.20-0.25) (Figs. S50, S51). The identity of the radioactive complex [^{89}Zr]Zr-TRITA was further confirmed by comparing its radio-HPLC elution profile to the UV-HPLC spectrum of nonradioactive ^{Nat}Zr-TRITA (Fig. S52).

Radiochemical Synthesis of [^{89}Zr]Zr-TETA with [^{89}Zr]$ZrCl_4$:

Complexing ^{89}Zr with the tetraazamacrocyclic ligand TETA was achieved by reacting 10-50 μg (10-50 μL, 1.0 mg/mL in water) of ligand TETA with an aliquot of [^{89}Zr]$ZrCl_4$ (0.4 - 0.5 mCi, 16.6 - 20.5 MBq) diluted in 200 μL of 0.5 M HEPES (pH 7.1-7.3) followed by 120 min incubation at 99 ºC in a thermomixer (550 rpm). The results of radiochemistry studies with different reaction buffers are summarized in Table S21. Formation of [^{89}Zr]Zr-TETA complex was monitored by radio-TLC using a mobile phase consisting of 50 mM EDTA (pH 5) on Varian ITLC-SA strips. In this ITLC-SA system, free ^{89}Zr formed a complex with EDTA and eluted with the solvent front (R_f ~ 1), while [^{89}Zr]Zr-TETA complex remained at the origin (R_f ~ 0) (Figs. S53).

Determination of Partition Coefficients (LogP).

The partition coefficient (logP) for each complex was determined by adding 5 μL of each [^{89}Zr]Zr-labeled complex (approx. 5 μCi; 0.19 MBq) to a mixture of 500 μL of octanol and 500 μL of water (pH 5.5).[65] The resulting solutions (n = 5) were vigorously vortexed for 5 min at room temperature, then centrifuged for 5 min to ensure complete separation of layers. From each of the five sets, 50 μL aliquot was removed from each phase into screw tubes and counted separately in a gamma counter. Each organic phase was washed with water to remove any radioactivity remaining in the organic phase before gamma counting. The partition coefficient was calculated as a ratio of counts in the octanol fraction to counts in the water fraction. The logP values were reported in an average of five measurements.

In vitro EDTA Challenge Study.

In vitro EDTA challenge study was carried out by adding 20 μL of each [^{89}Zr]Zr-labeled complex (110-120 μCi, 4.07-4.44 MBq) to 500 μL of EDTA (10 mM, 50 mM and 100 mM: pH 5 and pH 7) with a 1:100, 1:500, and 1:1000 ratio of ligand/EDTA.[15] The solutions (n=3) were incubated at 37 °C for 7 days in a thermomixer. Samples were analyzed at 0, 1, 3, 5, and 7 days post administration to EDTA by radio-TLC using Varian ITLC-SA strips and 50 mM EDTA (pH 5) as the mobile phase and gamma counting using an energy window of 500-1500 keV and standard protocols. All studies were performed in triplicate.

In vitro Metal Competition Study.

To a solution of metal cations [iron (III) chloride, cobalt (II) chloride, zinc (II) chloride, copper (II) chloride, magnesium (II) chloride, gallium (III) nitrate, gadolinium (III) chloride] (1 mM, 200 μL), was added [^{89}Zr]Zr-labeled complex (0.1 mM, 20 μL, 110-120 μCi, 4.07-4.44 MBq) in PBS, pH 7.4.[15] The resulting solutions (n = 3) were incubated at 37ºC for 7 days in a thermomixer. Dissociation of ^{89}Zr from [^{89}Zr]Zr-complexes was monitored by radio-TLC at 0, 1, 3, 5, and 7 days by radio - TLC using Varian ITLC-SA strips and 50 mM EDTA (pH 5) as the mobile phase and gamma counting using an energy window of 500-1500 keV and standard protocols. All studies were performed in triplicate.

In Vitro Serum Stability.

In vitro serum stability was carried out by adding 20 μL of each [^{89}Zr]Zr-labeled complex (110-120 μCi, 4.07-4.44 MBq) to 500 μL of human serum.[15] The solutions (n=3) were incubated at 37 °C for 7 days and were analyzed at 1, 3, 5, and 7 days by size exclusion chromatography (SEC) using a Superdex 200 10/300 GL™ column (GE Healthcare Life Sciences, Piscataway, NJ) and phosphate buffered saline (PBS) as eluent with a flow rate of 0.5 mL/min. Fractions (0.5 mL per tube) were collected and the activity in each fraction was measured in a gamma counter. The percent intact radiopharmaceutical was determined by subtracting the total integrated area under the product peak from the total integrated area generated for all peaks in the chromatogram and multiplying by a factor of 100%.

Biodistribution Studies.

Biodistribution studies were conducted using a modified literature procedure.[15] Briefly, female NIH Swiss mice (6-8 wk old, n=6) were injected with each [^{89}Zr]Zr-labeled complex (0.55 MBq (15 μCi)/mouse) via the tail vein, and sacrificed at 2, 4, 24, 48, 72 h post-injection. Organs and tissues of interest were excised, weighted, and counted on a Perkin Elmer 2480 Wizard® gamma counter (Waltham, MA). The percent injected dose per gram (%ID/g) and percent injected dose per organ (%ID/organ) were calculated by comparison to a weighed, counted standard for each group (Tables S23 - S25). The change in tissue associated activity over time was calculated using the formula: % 2h tissue-associated activity remaining at 72 h = 100 x [% ID/g_{72h} /%ID/$g_{2\ h}$].

Small Animal Models and PET Imaging.

Initial distribution and pharmacokinetics of the [^{89}Zr]Zr-PCTA or [^{89}Zr]Zr-NOTA in healthy NIH Swiss mice (n = 3/group) was recorded by dynamic PET scans (30 μg, 11.1 MBq) for 1 hour post-injection.[15] Dynamic PET scans were acquired in list mode format over 60 min, starting just prior to radiotracer injection. The resulting data was sorted into 0.5-mm sinogram bins and 60 time frames for image reconstruction (1 × 60 s). A microPET Focus 120 scanner (Concorde Microsystems, Knoxville, Tennessee) was used to obtain static scans at the desired time points with at least 10 million coincident events and ASIPro VM software was used to analyze acquired images. ROIs were drawn manually over the heart, liver, and kidneys (individually) and raw counts were adjusted to %-injected dose/gram via decay-corrected doses of [^{89}Zr]Zr-PCTA and [^{89}Zr]Zr-NOTA.

Dosimetry.

Biodistribution data from ex vivo studies, along with organ mass data collected during counting, were used to compute the fraction of administered activity in each tissue structure at 2 h, 4 h, 24 h, 48 h, and 72 h post-injection. Time-activity curves were integrated using the trapezoidal method with assumptions of constant uptake between 0 hours and 2 hours, and only physical decay beyond 72 hours. The resulting time-integrated activity coefficients (TIACs) were used to calculate tissue dosimetry using the OLIDNA/EXM v2.1 software platform. Based on typical animal weights for 6-8 week old female NIH Swiss mice, the 25 gram mouse phantom model was selected for calculations. A TIAC for the total body/remainder category was calculated by mono-exponential fitting to the aggregate organ clearance data, followed by applying the obtained exponential rate constant to the otherwise un-accounted for administered activity. The urinary bladder contents residence was calculated using the same whole-body clearance rate, assuming a voiding interval of 0.1 hours. Resultant dosimetric data are presented with units of absorbed dose (mGy/MBq) rather than equivalent dose (mSv/MBq) to avoid confusion regarding the concept of effective dose or effective dose equivalent in mice. With that said, all radiation from ^{89}Zr is assumed to have a radiation-specific weighting factor of 1, and thus the conversion from absorbed dose to equivalent dose would also be a factor of 1.

Supplementary Material

Refer to Web version on PubMed Central for supplementary material.

ACKNOWLEDGMENT

The authors acknowledge support from the University of Iowa, Wake Forest University Health Sciences, Wake Forest Innovations, and the North Carolina Biotechnology Center (2016-BIG-6524). High-resolution mass spectrometry was provided by the Mass Spectrometry Core Laboratory at the University of North Carolina at Chapel Hill. X-ray facilities at Wake Forest University are supported in part by the National Science Foundation (CHE-0234489). We gratefully acknowledge Marcus Wright, Ph.D. for NMR analysis. We gratefully acknowledge the Small Animal Imaging and the Radiochemistry and Molecular Imaging Probe Core Facilities at MSK, all of which are supported in part by NIH grant P30 CA08748. We acknowledge the Center for Molecular Imaging and Nanotechnology (CMINT) Tow Fellowship through MSK (K.E.H.). We would also like to acknowledge financial support from R35 CA232130 (J.S.L.).

T.J.W., D.N.P. and N.B. have been awarded patents WO2017161356A1 and WO2019/147912A1 relating to this work. All other authors declare no competing financial interests exist.

REFERENCES

(1). Van Dongen GA; Huisman MC; Boellaard R; Harry Hendrikse N; Windhorst AD; Visser GW; Molthoff CF; Vugts DJ ^{89}Zr-immuno-PET for imaging of long circulating drugs and disease targets: why, how and when to be applied? Q J Nucl Med Mol Imaging 2015, 59, 18–38. [PubMed: 25517081]

(2). van Dongen GA; Visser GW; Lub-de Hooge MN; de Vries EG; Perk LR Immuno-PET: a navigator in monoclonal antibody development and applications. Oncologist 2007, 12, 1379–1389. [PubMed: 18165614]

(3). Wright BD; Lapi SE Designing the magic bullet? The advancement of immuno-PET into clinical use. J Nucl Med 2013, 54, 1171–1174. [PubMed: 23908265]

(4). Jauw YW; Menke-van der Houven van Oordt CW; Hoekstra OS; Hendrikse NH; Vugts DJ; Zijlstra JM; Huisman MC; van Dongen GA Immuno-Positron Emission Tomography with Zirconium-89-

Labeled Monoclonal Antibodies in Oncology: What Can We Learn from Initial Clinical Trials? Front Pharmacol 2016, 7, 131. [PubMed: 27252651]

(5). Cornelis FH; Durack JC; Pandit-Taskar N; Ulaner GA; Lewis JS; Morris MJ; Solomon SB Long-Half-Life (89)Zr-Labeled Radiotracers Can Guide Percutaneous Biopsy Within the PET/CT Suite Without Reinjection of Radiotracer. J Nucl Med 2018, 59, 399–402. [PubMed: 28818992]

(6). Henry KE; Ulaner GA; Lewis JS Human Epidermal Growth Factor Receptor 2-Targeted PET/Single-Photon Emission Computed Tomography Imaging of Breast Cancer: Noninvasive Measurement of a Biomarker Integral to Tumor Treatment and Prognosis. PET Clin 2017, 12, 269–288. [PubMed: 28576166]

(7). Henry KE; Ulaner GA; Lewis JS Clinical Potential of Human Epidermal Growth Factor Receptor 2 and Human Epidermal Growth Factor Receptor 3 Imaging in Breast Cancer. PET Clin 2018, 13, 423–435. [PubMed: 30100080]

(8). Ulaner GA; Carrasquillo JA; Riedl CC; Yeh R; Hatzoglou V; Ross DS; Jhaveri K; Chandarlapaty S; Hyman DM; Zeglis BM; Lyashchenko SK; Lewis JS Identification of HER2-Positive Metastases in Patients with HER2-Negative Primary Breast Cancer by Using HER2-targeted (89)Zr-Pertuzumab PET/CT. Radiology 2020, 296, 370–378. [PubMed: 32515679]

(9). Ulaner GA; Hyman DM; Lyashchenko SK; Lewis JS; Carrasquillo JA ^{89}Zr-Trastuzumab PET/CT for Detection of Human Epidermal Growth Factor Receptor 2-Positive Metastases in Patients With Human Epidermal Growth Factor Receptor 2-Negative Primary Breast Cancer. Clin Nucl Med 2017, 42, 912–917. [PubMed: 28872549]

(10). Ulaner GA; Hyman DM; Ross DS; Corben A; Chandarlapaty S; Goldfarb S; McArthur H; Erinjeri JP; Solomon SB; Kolb H; Lyashchenko SK; Lewis JS; Carrasquillo JA Detection of HER2-Positive Metastases in Patients with HER2-Negative Primary Breast Cancer Using ^{89}Zr-Trastuzumab PET/CT. J Nucl Med 2016, 57, 1523–1528. [PubMed: 27151988]

(11). Ulaner GA; Lyashchenko SK; Riedl C; Ruan S; Zanzonico PB; Lake D; Jhaveri K; Zeglis B; Lewis JS; O'Donoghue JA First-in-Human Human Epidermal Growth Factor Receptor 2-Targeted Imaging Using (89)Zr-Pertuzumab PET/CT: Dosimetry and Clinical Application in Patients with Breast Cancer. J Nucl Med 2018, 59, 900–906. [PubMed: 29146695]

(12). Bhatt NB; Pandya DN; Wadas TJ Recent advances in zirconium-89 chelator development. Molecules 2018, 23, 638/631–638.

(13). Deri MA; Zeglis BM; Francesconi LC; Lewis JS PET imaging with (8)(9)Zr: from radiochemistry to the clinic. Nucl Med Biol 2013, 40, 3–14. [PubMed: 22998840]

(14). Price EW; Orvig C Matching chelators to radiometals for radiopharmaceuticals. Chem Soc Rev 2014, 43, 260–290. [PubMed: 24173525]

(15). Pandya DN; Bhatt N; Yuan H; Day CS; Ehrmann BM; Wright M; Bierbach U; Wadas TJ Zirconium tetraazamacrocycle complexes display extraordinary stability and provide a new strategy for zirconium-89-based radiopharmaceutical development. Chem. Sci 2017, 8, 2309–2314. [PubMed: 28451334]

(16). Houghton JL; Zeglis BM; Abdel-Atti D; Sawada R; Scholz WW; Lewis JS Pretargeted Immuno-PET of Pancreatic Cancer: Overcoming Circulating Antigen and Internalized Antibody to Reduce Radiation Doses. J Nucl Med 2016, 57, 453–459. [PubMed: 26471693]

(17). Zeglis BM; Davis CB; Abdel-Atti D; Carlin SD; Chen A; Aggeler R; Agnew BJ; Lewis JS Chemoenzymatic strategy for the synthesis of site-specifically labeled immunoconjugates for multimodal PET and optical imaging. Bioconjug Chem 2014, 25, 2123–2128. [PubMed: 25418333]

(18). Zeglis BM; Davis CB; Aggeler R; Kang HC; Chen A; Agnew BJ; Lewis JS Enzyme-mediated methodology for the site-specific radiolabeling of antibodies based on catalyst-free click chemistry. Bioconjug Chem 2013, 24, 1057–1067. [PubMed: 23688208]

(19). Zeglis BM; Emmetiere F; Pillarsetty N; Weissleder R; Lewis JS; Reiner T Building Blocks for the Construction of Bioorthogonally Reactive Peptides via Solid-Phase Peptide Synthesis. ChemistryOpen 2014, 3, 48–53. [PubMed: 24808990]

(20). Zeglis BM; Lewis JS The bioconjugation and radiosynthesis of ^{89}Zr-DFO-labeled antibodies. J Vis Exp 2015.

(21). Mckinght BN; Viola-Villegas NT ^{89}Zr-ImmunoPET comapnion diagnostics and their impact on clinical drug development. J Labelled Compd Rad 2018, 727–738.

(22). Carmon KS; Azhdarinia A Application of Immuno-PET in Antibody-Drug Conjugate Development. Mol Imaging 2018, 17, 1–10.

(23). Bhatt NB; Pandya DN; Rideout-Danner S; Gage HD; Marini FC; Wadas TJ A comprehensively revised strategy that improves the specific activity and long-term stability of clinically relevant ^{89}Zr-immuno-PET agents. Dalton Trans. 2018, 47, 13214–13221. [PubMed: 30178793]

(24). Pandya DN; Bhatt NB; Almaguel F; Rideout-Danner S; Gage HD; Sai KKS; Wadas TJ ^{89}Zr-chloride can be used for immuno-PET radiochemistry without loss of antigen reactivity in vivo. J. Nucl. Med 2019, 60, 696–701. [PubMed: 30442753]

(25). Wadas TJ; Wong EH; Weisman GR; Anderson CJ Coordinating radiometals of copper, gallium, indium, yttrium, and zirconium for PET and SPECT imaging of disease. Chem Rev 2010, 110, 2858–2902. [PubMed: 20415480]

(26). Price TW; Greenman J; Stasiuk GJ Current advances in ligand design for inorganic positron emission tomography tracers (68)Ga, (64)Cu, (89)Zr and (44)Sc. Dalton Trans 2016, 45, 15702–15724. [PubMed: 26865360]

(27). Allott L; Da Pieve C; Meyers J; Spinks T; Ciobota DM; Kramer-Marek G; Smith G Evaluation of DFO-HOPO as an octadentate chelator for zirconium-89. Chem Commun 2017, 53, 8529–8532.

(28). Alnahwi AH; Ait-Mohand S; Dumulon-Perreault V; Dory YL; Guerin B Promising Performance of 4HMS, a New Zirconium-89 Octadendate Chelator. ACS Omega 2020, 5, 10731–10739. [PubMed: 32455192]

(29). Bhatt NB; Pandya DN; Wadas TJ; Xu J; Tatum D; Magda D Evaluation of macrocyclic hydroxyisophthalamide ligands as chelators for zirconium-89. PLoS One 2017, 12, e0178767. [PubMed: 28575044]

(30). Boros E; Holland JP; Kenton N; Rotile N; Caravan P Macrocycle-Based Hydroxamate Ligands for Complexation and Immunoconjugation of (89)Zirconium for Positron Emission Tomography (PET) Imaging. Chempluschem 2016, 81, 274–281. [PubMed: 27630807]

(31). Deri MA; Ponnala S; Zeglis BM; Pohl G; Dannenberg JJ; Lewis JS; Francesconi LC Alternative chelator for (8)(9)Zr radiopharmaceuticals: radiolabeling and evaluation of 3,4,3-(LI-1,2-HOPO). J Med Chem 2014, 57, 4849–4860. [PubMed: 24814511]

(32). Glassner M; Palmieri L; Monnery BD; Verbrugghen T; Deleye S; Stroobants S; Staelens S; Wyffels L; Hoogenboom R The Label Matters: muPET Imaging of the Biodistribution of Low Molar Mass (89)Zr and (18)F-Labeled Poly(2-ethyl-2-oxazoline). Biomacromolecules 2017, 18, 96–102. [PubMed: 28064503]

(33). Guerard F; Lee Y-S; Brechbiel MW Rational Design, Synthesis, and Evaluation of Tetrahydroxamic Acid Chelators for Stable Complexation of Zirconium(IV). Chem. - Eur. J 2014, 20, 5584–5591. [PubMed: 24740517]

(34). Pandya DN; Pailloux S; Tatum D; Magda D; Wadas TJ Di-macrocyclic terephthalamide ligands as chelators for the PET radionuclide zirconium-89. Chem. Commun 2015, 51, 2301–2303.

(35). Price EW; Zeglis BM; Lewis JS; Adam MJ; Orvig C H6phospa-trastuzumab: bifunctional methylenephosphonate-based chelator with ^{89}Zr, ^{111}In and ^{177}Lu. Dalton Trans 2014, 43, 119–131. [PubMed: 24104523]

(36). Rudd SE; Roselt P; Cullinane C; Hicks RJ; Donnelly PS A desferrioxamine B squaramide ester for the incorporation of zirconium-89 into antibodies. Chem Commun 2016, 52, 11889–11892.

(37). Sarbisheh EK; Salih AK; Raheem SJ; Lewis JS; Price EW A High-Denticity Chelator Based on Desferrioxamine for Enhanced Coordination of Zirconium-89. Inorg Chem 2020, 59, 16, 11715–11727. [PubMed: 32799484]

(38). Tinianow JN; Pandya DN; Pailloux SL; Ogasawara A; Vanderbilt AN; Gill HS; Williams S-P; Wadas TJ; Magda D; Marik J Evaluation of a 3-hydroxypyridin-2-one (2,3-HOPO) based macrocyclic chelator for $^{89}Zr^{4+}$ and its use for immunoPET imaging of HER2 positive model of ovarian carcinoma in mice. Theranostics 2016, 6, 511–521. [PubMed: 26941844]

(39). Vugts DJ; Klaver C; Sewing C; Poot AJ; Adamzek K; Huegli S; Mari C; Visser GW; Valverde IE; Gasser G; Mindt TL; van Dongen GA Comparison of the octadentate bifunctional chelator

DFO*-pPhe-NCS and the clinically used hexadentate bifunctional chelator DFO-pPhe-NCS for (89)Zr-immuno-PET. Eur J Nucl Med Mol Imaging 2017, 44, 286–295. [PubMed: 27573793]

(40). Zhai C; Summer D; Rangger C; Franssen GM; Laverman P; Haas H; Petrik M; Haubner R; Decristoforo C Novel Bifunctional Cyclic Chelator for (89)Zr Labeling-Radiolabeling and Targeting Properties of RGD Conjugates. Mol Pharm 2015, 12, 2142–2150. [PubMed: 25941834]

(41). Alves LG; Hild F; Munha RF; Veiros LF; Dagorne S; Martins AM Synthesis and structural characterization of novel cyclam-based zirconium complexes and their use in the controlled ROP of rac-lactide: access to cyclam-functionalized polylactide materials. Dalton Trans 2012, 41, 14288–14298. [PubMed: 23041769]

(42). Alves LG; Madeira F; Munha RF; Barroso S; Veiros LF; Martins AM Reactions of heteroallenes with cyclam-based Zr(IV) complexes. Dalton Trans 2015, 44, 1441–1455. [PubMed: 25427676]

(43). Munha RF; Veiros LF; Duarte MT; Fryzuk MD; Martins AM Synthesis and structural studies of amido, hydrazido and imido zirconium(IV) complexes incorporating a diamido/diamine cyclam-based ligand. Dalton Transactions 2009, 7494–7508. [PubMed: 19727472]

(44). Jewula P; Berthet JC; Chambron JC; Rousselin Y; Thuery P; Meyer M Synthesis and Structural Study of Tetravalent (Zr^{4+}, Hf^{4+}, Ce^{4+}, Th^{4+}, U^{4+}) Metal Complexes with Cyclic Hydroxamic Acids. Eur J Inorg Chem 2015, 1529–1541.

(45). Li AK; Ma HY; Huang JL Zirconium complexes bearing bis(phenoxy-imine) ligands with bulky o-bis(aryl)methyl-substituted aniline groups: synthesis, characterization and ethylene polymerization behavior. Appl Organomet Chem 2013, 27, 341–347.

(46). DeAngelis S; Solari E; Floriani C; Chiesi-Villa A; Rizzoli C Mono- and bis(dibenzotetramethyltetraaza[14]annulene) complexes of Group IV metals including the structure of the lithium derivative of the macrocyclic ligand. Inorg Chem 1992, 31, 2520–2527.

(47). Rogers AJ; Solari E; Floriani C; ChiesiVilla A; Rizzoli C New directions in amido-transition metal chemistry: The preparation and reaction of mixed amino-amido macrocyclic ligands. J Chem Soc Dalton Trans 1997, 2385–2386.

(48). Solari E; Maltese C; Franceschi F; Floriani C; ChiesiVilla A; Rizzoli C Geometrical isomerism and redox behaviour in zirconium-Schiff base complexes: the formation of C-C bonds functioning as two-electron reservoirs. J Chem Soc Dalton Trans 1997, 2903–2910.

(49). Solari G; Solari E; Floriani C; ChiesiVilla A; Rizzoli C Bifunctional carriers of alkali-metal enolates: The use of zirconium meso-octaethylporphyrinogen in aldol condensation reactions. Organometallics 1997, 16, 508–510.

(50). Kato CN; Shinohara A; Hayashi K; Nomiya K Syntheses and X-ray crystal structures of zirconium(IV) and hafnium(IV) complexes containing monovacant Wells-Dawson and Keggin polyoxotungstates. Inorg Chem 2006, 45, 8108–8119. [PubMed: 16999408]

(51). Wang GC; Sung HH; Williams ID; Leung WH Tetravalent titanium, zirconium, and cerium oxo and peroxo complexes containing an imidodiphosphinate ligand. Inorg Chem 2012, 51, 3640–3647. [PubMed: 22376219]

(52). Howard WA; Waters M; Parkin G Terminal zirconium Oxo complexes: synthesis, structure and reactivity of (n^5-$C_5Me_4R)_2Zr(O)(NC_5H_4R'$). J Am Chem Soc 1993, 115, 4917–4918.

(53). Hollink E; Stephan DW Zirconium and hafnium. ChemInform 2004, 35, 106–160.

(54). Page EM; Wass SA Zirconium and hafnium 1994. Coord Chem Rev 1996, 152, 411–466.

(55). Hohenstein EG; Sherrill CD Effects of heteroatoms on aromatic pi-pi interactions: benzene-pyridine and pyridine dimer. J Phys Chem A 2009, 113, 878–886. [PubMed: 19132847]

(56). Mishra PK; Sathyamurthy N pi-pi-interactionsin pyridine. J Phys Chem Lett A 2005, 109, 6–8.

(57). Alam MA; Nethaji M; Ray M Structural characterization of an enantiopure hydroxo-bridged binuclear iron(III) complex with empty one-dimensional helical channels. Inorg Chem 2005, 44, 1302–1308. [PubMed: 15732970]

(58). Berry JF; Bill E; Garcia-Serres R; Neese F; Weyhermuller T; Wieghardt K Effect of N-methylation of macrocyclic amine ligands on the spin state of iron(III): a tale of two fluoro complexes. Inorg Chem 2006, 45, 2027–2037. [PubMed: 16499363]

(59). Balogh E; Tripier R; Ruloff R; Toth E Kinetics of formation and dissociation of lanthanide(III) complexes with the 13-membered macrocyclic ligand TRITA^{4-}. Dalton Trans 2005, 1058–1065. [PubMed: 15739008]

(60). Marques F; Gano L; Paula Campello M; Lacerda S; Santos I; Lima LM; Costa J; Antunes P; Delgado R 13- and 14-membered macrocyclic ligands containing methylcarboxylate or methylphosphonate pendant arms: chemical and biological evaluation of their (153)Sm and (166)Ho complexes as potential agents for therapy or bone pain palliation. J Inorg Biochem 2006, 100, 270–280. [PubMed: 16387365]

(61). Spirlet MR; REbisant J; Loncin MF; Desreux JF Structural characterization of a terbium(III) complex with 1,4,8,11-tetraazacyclotetradecane-1,4,8,11-tetraacetic acid. Lanthanide ions and the conformation of the 14-membered macrocycles. Inorg Chem 1984, 23, 4278–4283.

(62). Kumar KM; Tweedle MF; Malley MF; Gougoutas JZ Synthesis, Stability, and Crystal Structure Studies of Some Ca^{2+}, Cu^{2+}, and Zn^{2+} Complexes of Macrocyclic Polyamino Carboxylates. Inorg Chem 1995, 34, 6472–6480.

(63). Maurya MR; Zaluzec EJ; Pakovic SF; Herlinger AW Alkaline-earth-metal complexes of 1,4,8,11-tetraazacyclotetradecane-1,4,8,11-tetraacetic acid, H_4TETA, and crystal and molecular structure of H_4TETA.cntdot·6H_2O and [Mg(H_2TETA)($H_2O)_4$].cntdot·4H_2O. Inorg Chem 1991, 30, 3657–3662.

(64). Hancock RD Chelate Ring Size and Metal Ion Selection. J Chem Ed 1992, 69, 615–621.

(65). Waterhouse RN Determination of lipophilicity and its use as a predictor of blood-brain barrier penetration of molecular imaging agents. Mol Imaging Biol 2003, 5, 376–389. [PubMed: 14667492]

(66). Meneton P; Ichikawa I; Inagami T; Schnermann J Renal physiology of the mouse. Am J Physiol Renal Physiol 2000, 278, F339–351. [PubMed: 10710537]

(67). Schock-Kusch D; Geraci S; Ermeling E; Shulhevich Y; Sticht C; Hesser J; Stsepankou D; Neudecker S; Pill J; Schmitt R; Melk A Reliability of transcutaneous measurement of renal function in various strains of conscious mice. PLoS One 2013, 8, e71519. [PubMed: 23977062]

(68). Ferreira CL; Lamsa E; Woods M; Duan Y; Fernando P; Bensimon C; Kordos M; Guenther K; Jurek P; Kiefer GE Evaluation of bifunctional chelates for the development of gallium-based radiopharmaceuticals. Bioconjug Chem 2010, 21, 531–536. [PubMed: 20175523]

(69). Holub J; Meckel M; Kubicek V; Rosch F; Hermann P Gallium(III) complexes of NOTA-bis (phosphonate) conjugates as PET radiotracers for bone imaging. Contrast Media Mol Imaging 2015, 10, 122–134. [PubMed: 24801892]

(70). Kubicek V; Bohmova Z; Sevcikova R; Vanek J; Lubal P; Polakova Z; Michalicova R; Kotek J; Hermann P NOTA Complexes with Copper(II) and Divalent Metal Ions: Kinetic and Thermodynamic Studies. Inorg Chem 2018, 57, 3061–3072. [PubMed: 29488748]

(71). Bruker APEX2 2014.11-0 ed.; Bruker AXS Inc.: Madison, Wisconsin, USA, 2014.

(72). SAINT 8.34A ed.; Bruker AXS Inc.: Madison, Wisconsin, USA, 2014.

(73). Bruker APEX3 2016.1-0 ed.; Bruker AXS Inc.: Madison, Wisconsin, USA., 2016.

(74). Sheldrick GM; SHELXL, 2014/7 ed.; Bruker AXS Inc.: Madison, Wisconsin, USA., 2014.

(75). Sheldrick GM A short history of SHELX. Acta Crystallography 2008, A64, 112–122.

(76). Sheldrick GM; SADABS, 2014/5 ed. University of Göttingen, Germany, 2014.

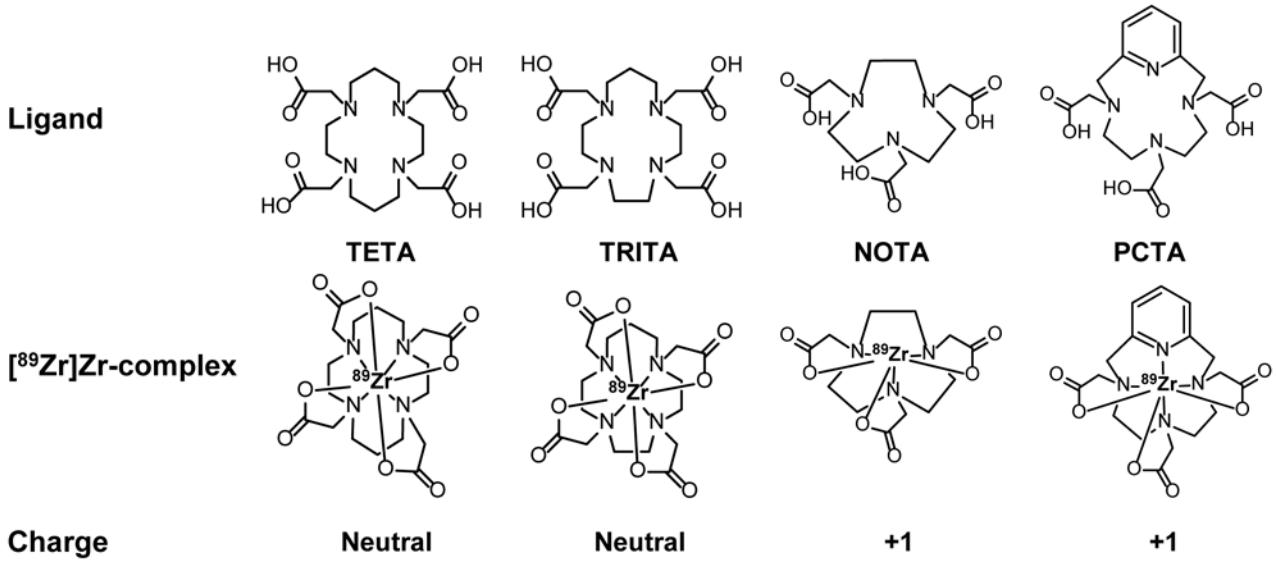

Figure 1.
Structures of polyazamacrocyclic ligands and their ^{89}Zr-complexes.

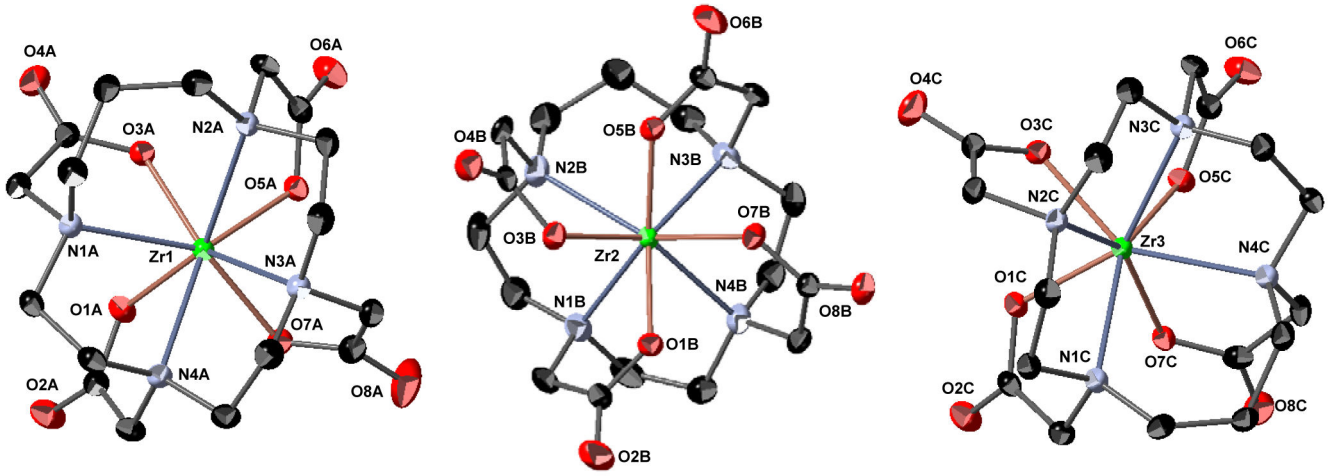

Figure 2.

The crystal structure of $[Zr(C_{17}H_{26}N_4O_8)] - 3.33\ H_2O$ (Zr-TRITA). The asymmetric unit cell contains three crystallographically-independent molecules. The introduction of the additional methylene unit into the TRITA backbone increases the *cis*-N-Zr-N bite angle of the cyclam portion of the ligand by 15° when compared to the *cis*-N-Zr-N bite angle exhibited by the cyclen portion of the ligand. Only a partial numbering scheme is provided. Solvent molecules and hydrogen atoms are omitted for clarity. Thermal ellipsoids are drawn at the 50% probability level.

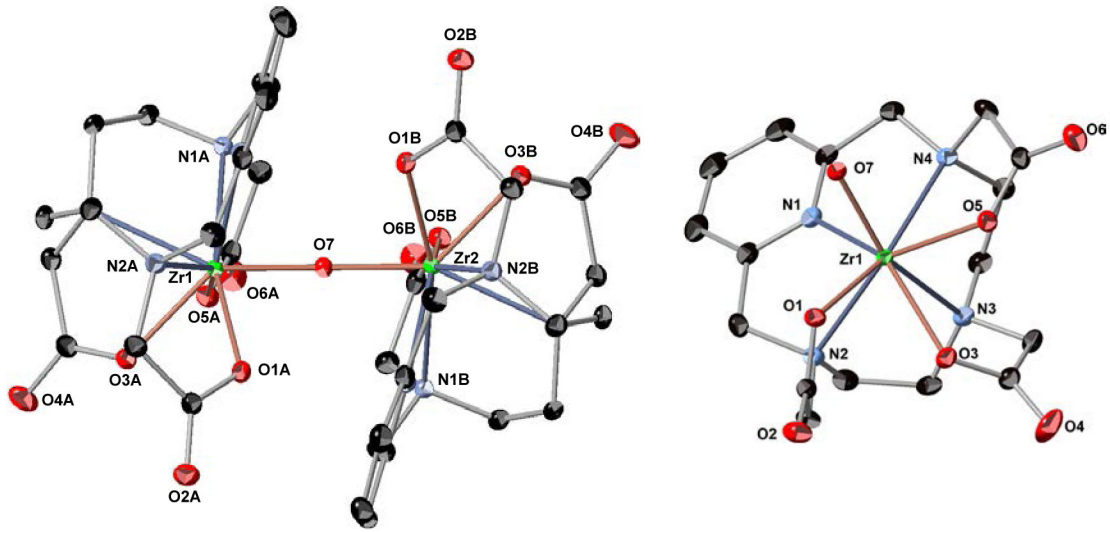

Figure 3.

Crystal structure of $[Zr(C_{17}H_{21}N_4O_6)]_2O$ - 8 H_2O (Zr-PCTA). (Left) The seven coordinate monomers are bridged by one oxygen atom, which lies on the crystallographic 2-fold axis at ½, y, ¼ in the unit cell, to fulfill Zr^{4+} ion's requirement of an octa-coordinate ligand sphere. (Right) The monomer is depicted so that the coordination sphere around the Zr^{4+} ion is visualized more easily. Nitrogen one (N1) represents the nitrogen atom of the pyridyl ring. Only a partial numbering scheme is provided. Solvent molecules and hydrogen atoms are omitted for clarity. Thermal ellipsoids are drawn at the 50% probability level. The molecules are labeled to facilitate the identification of the symmetry related atoms only.

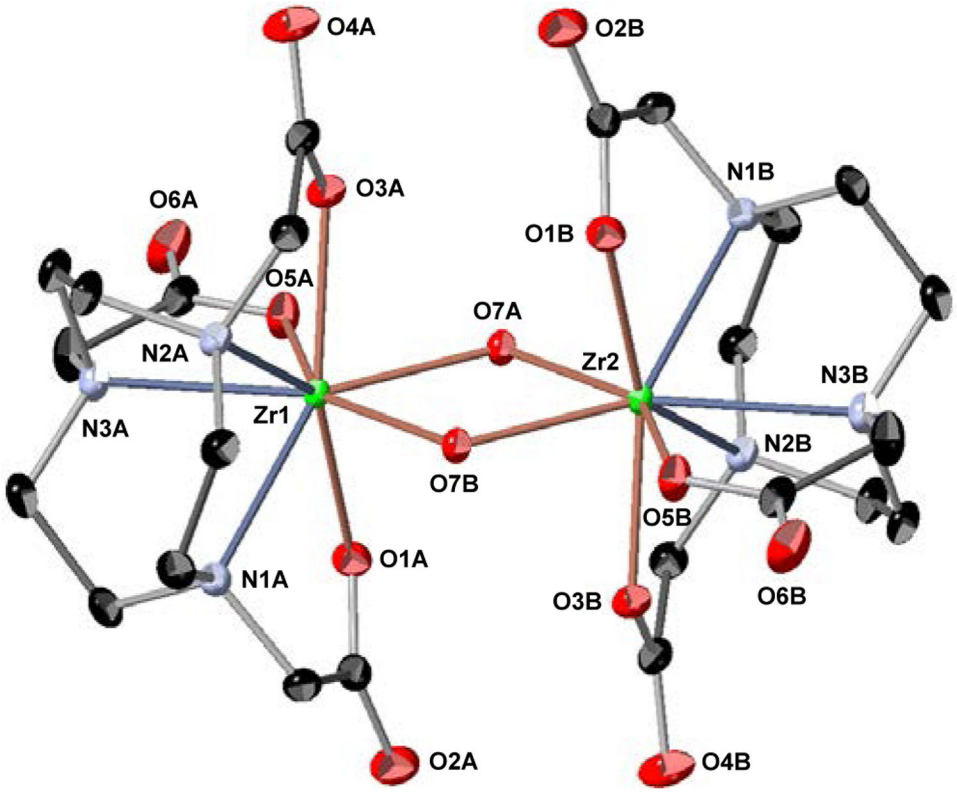

Figure 4.

Crystal structure of $[Zr(C_{12}H_{18}N_3O_6)(OH)]_2$ - 6 H_2O (Zr-NOTA). Zr-NOTA crystalizes as a binuclear complex. The six coordinate monomers, which are defined by the Zr-NOTA subunits are bridged by two OH groups (O7A and O7B) and are related by the crystallographic inversion center at ½, ½, 0 in the unit cell. Only a partial numbering scheme is provided. Solvent molecules and hydrogen atoms are omitted for clarity. Thermal ellipsoids are drawn at the 50% probability level. The molecules are labeled to facilitate the identification of the symmetry related atoms only.

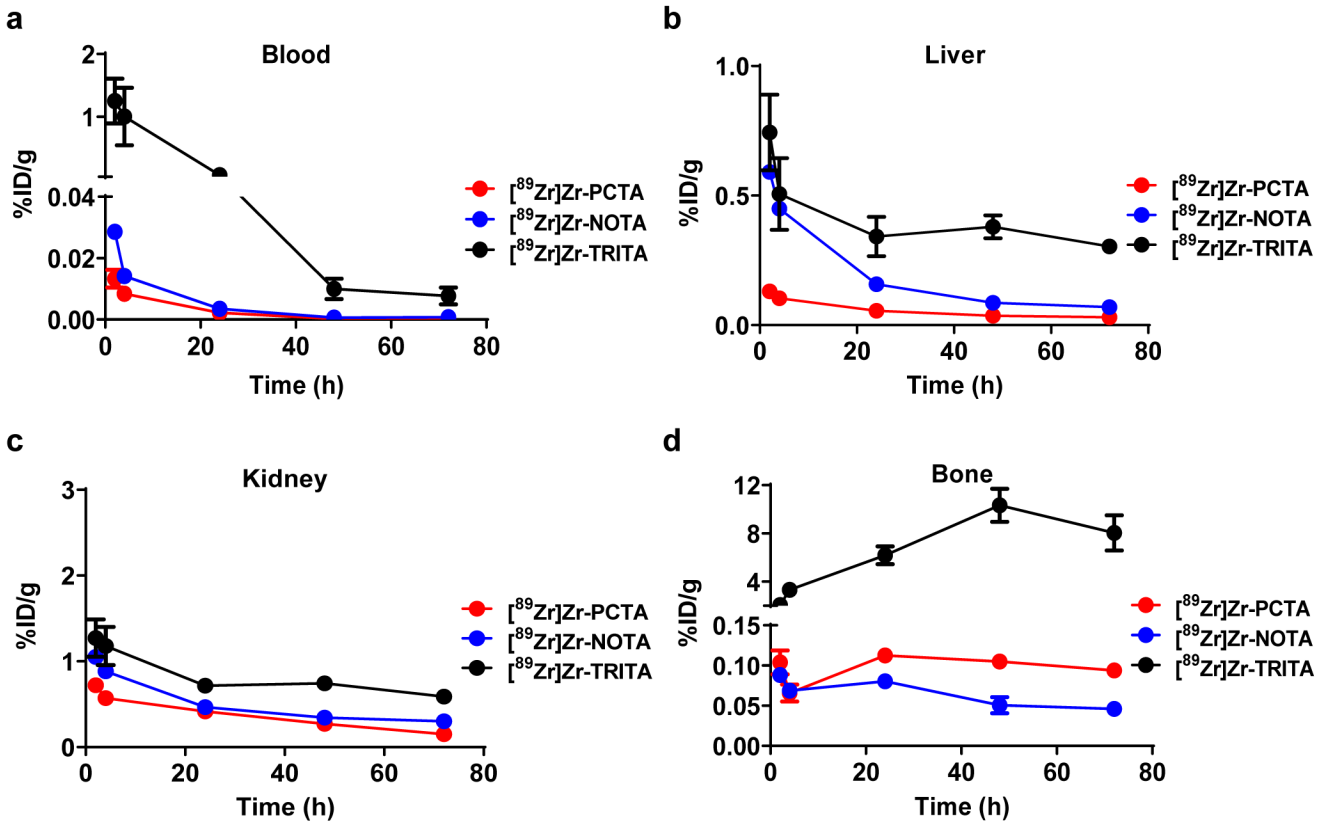

Figure 5.

Biodistribution data summary of [^{89}Zr]Zr-PCTA, [^{89}Zr]Zr-NOTA, and [^{89}Zr]Zr-TRITA in selected tissues: (a) blood, (b) liver, (c) kidney, and (d) bone. Based upon these studies [^{89}Zr]Zr-TRITA demonstrated the worst *in vivo* behavior of the three radiometal complexes. [^{89}Zr]Zr-PCTA and [^{89}Zr]Zr-NOTA demonstrated more efficient clearance profiles from tissue suggesting that their *in vivo* behavior is improved compared to that of [^{89}Zr]Zr-TRITA.

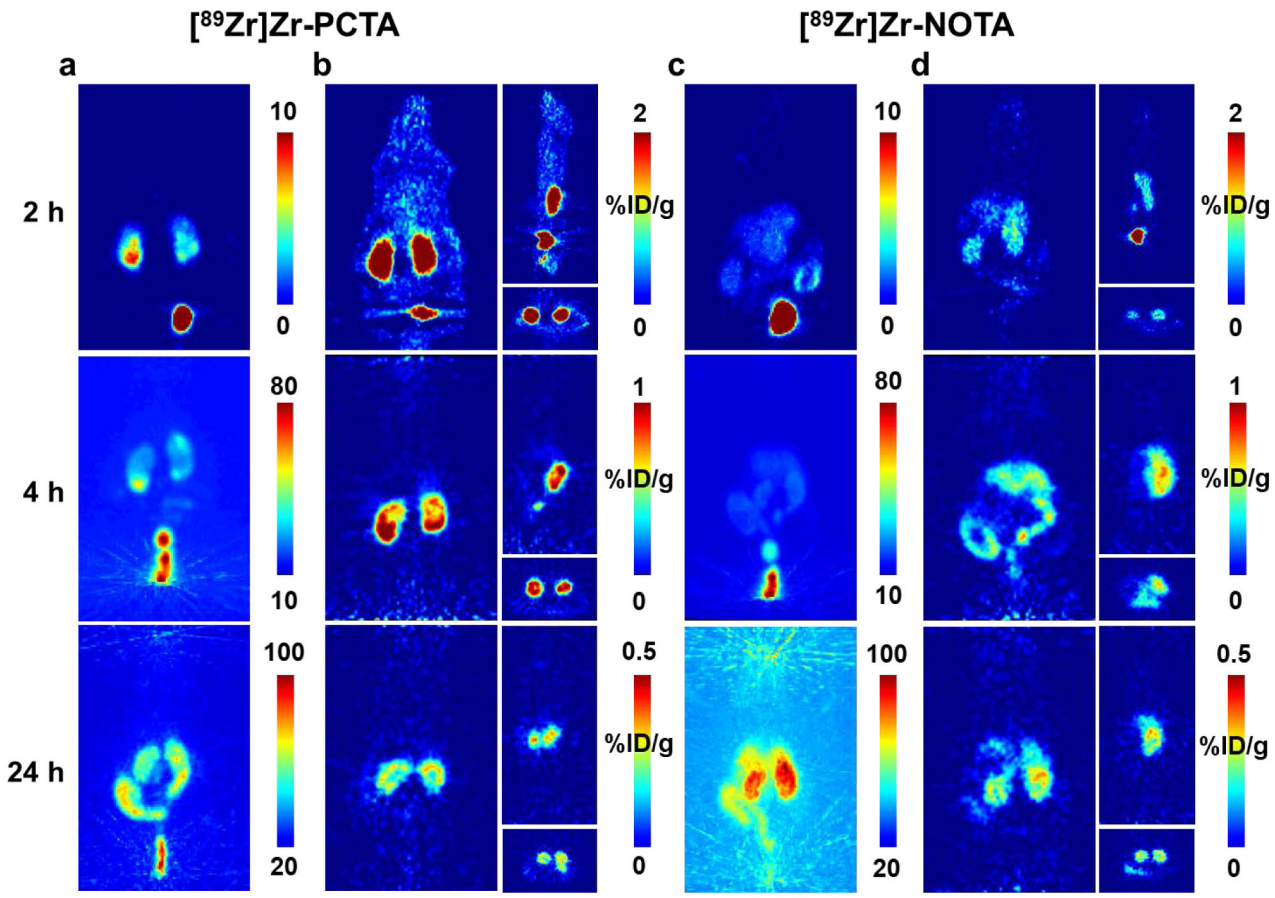

Figure 6.

Representative static PET images of [^{89}Zr]Zr-PCTA and [^{89}Zr]Zr-NOTA over 24 h. Panels a and c represent the maximum intensity projections for each radiometal complex, respectively. Panels b and d represent the coronal (left), sagittal (top right), and transverse (bottom right) views for each radiometal complex, respectively. Rapid clearance is observed at 2 h through bladder and kidneys, with increased accumulation in the kidneys over time and minimal uptake in non-clearance tissues at 24 h.

Table 1.

Summary of optimized radiochemistry conditions to prepare [^{89}Zr]Zr-complexes with [^{89}Zr]$ZrCl_4$

Radiochemistry conditions	Ligands (n = 30)			
	PCTA	**NOTA**	**TRITA**	**TETA**
Quantity (μg)	15-20	15-17	18-24	10-50
[^{89}Zr]$ZrCl_4$ added (MBq)	41.6-55.5	41.7-55.7	40.7-51.8	16.5-20.5
Reaction Buffer	0.5 M HEPES	0.5 M HEPES	0.5 M HEPES	0.5 M HEPES
Final Reaction pH	6.9-7.2	6.9-7.2	3.9-4.2	6.9-7.3
Reaction Temperature (°C)	37 [a]	37 [a]	180 [b]	99 [a]
Reaction time (min)	60	60	20	120
Radiochemical yield (%)	100	100	100	0
Molar activity (A_m; MBq μmol^{-1})	1035 ± 6	995 ± 7	890 ± 9	-

[a] Conventional heating.

[b] Microwave heating.

Table 2.

Chronological stability study of [^{89}Zr]Zr-complexes in EDTA (pH 5 and pH 7) challenge study maintained at 37°C for 7 days and analyzed by Radio-ITLC (n = 3 for each [^{89}Zr]Zr-complex at each pH and time point)

Complex	EDTA	pH	% Intact of [^{89}Zr]Zr-complexes (n = 3)				
			0 h	1 d	3 d	5 d	7 d
[^{89}Zr]Zr-PCTA	100-fold	7.0	**100**	**100**	**100**	**100**	**100**
		5.0	**100**	**100**	**100**	**100**	**100**
	500-fold	7.0	**100**	**100**	**100**	**100**	**100**
		5.0	**100**	**100**	**100**	**100**	**100**
	1000-fold	7.0	**100**	**100**	**100**	**100**	**100**
		5.0	**100**	**100**	**100**	**100**	**100**
[^{89}Zr]Zr-NOTA	100-fold	7.0	100	94.5 ± 0.5	85.3 ± 0.8	82.9 ± 0.7	80.8 ± 0.4
		5.0	100	93.0 ± 0.3	82.7 ± 0.7	80.3 ± 0.2	78.4 ± 0.6
	500-fold	7.0	100	93.1 ± 0.1	83.8 ± 0.7	81.2 ± 0.3	73.3 ± 1.4
		5.0	100	83.7 ± 1.3	75.8 ± 1.8	72.9 ± 1.2	71.2 ± 1.7
	1000-fold	7.0	100	93.1 ± 0.4	81.8 ± 1.6	76.7 ± 0.8	70.7 ± 1.0
		5.0	100	78.5 ± 0.7	71.8 ± 0.8	66.4 ± 1.0	65.3 ± 1.2
[^{89}Zr]Zr-TRITA	100-fold	7.0	99.4 ± 0.3	44.7 ± 0.8	20.5 ± 1.1	1.1 ± 0.5	0
		5.0	99.7 ± 0.2	85.7 ± 1.6	64.0 ± 1.4	40.5 ± 0.2	36.3 ± 0.4
	500-fold	7.0	99.4 ± 0.3	23.1 ± 1.2	3.8 ± 0.9	0	0
		5.0	99.7 ± 0.2	75.6 ± 1.0	45.5 ± 2.5	19.6 ± 0.6	16.7 ± 0.5
	1000-fold	7.0	99.4 ± 0.3	13.1 ± 0.9	1.9 ± 0.7	0	0
		5.0	99.7 ± 0.2	69.6 ± 0.7	35.8 ± 1.7	13.8 ± 3.5	9.6 ± 0.1

Table 3.

Chronological stability study of [^{89}Zr]Zr-complexes with various metals in competition study (PBS, pH 7.4) maintained at 37°C for 7 days and analyzed by Radio-ITLC (n = 3 for each [^{89}Zr]Zr-complex with each metal and time point)

Time Point	Complex	% Intact of [^{89}Zr]Zr-complexes (n = 3)						
		Fe^{3+}	Zn^{2+}	Co^{2+}	Cu^{2+}	Mg^{2+}	Gd^{3+}	Ga^{3+}
0 h	**[^{89}Zr]Zr-PCTA**	**100**	**100**	**100**	**100**	**100**	**100**	**100**
	[^{89}Zr]Zr-NOTA	100	100	100	100	100	100	100
	[^{89}Zr]Zr-TRITA	99.7 ± 0.2	99.6 ± 0.2	99.5 ± 0.2	99.7 ± 0.2	99.6 ± 0.2	99.5 ± 0.2	99.7 ± 0.2
1 d	**[^{89}Zr]Zr-PCTA**	**100**	**100**	**100**	**100**	**100**	**100**	**100**
	[^{89}Zr]Zr-NOTA	99.0 ± 0.1	96.1 ± 0.1	97.7 ± 0.4	96.1 ± 0.2	95.5 ± 0.3	98.3 ± 0.1	97.9 ± 0.1
	[^{89}Zr]Zr-TRITA	91.3 ± 0.3	29.2 ± 1.2	35.6 ± 2.3	94.5 ± 0.9	90.4 ± 1.0	88.7 ± 0.8	94.6 ± 0.8
3 d	**[^{89}Zr]Zr-PCTA**	**100**	**100**	**100**	**100**	**100**	**100**	**100**
	[^{89}Zr]Zr-NOTA	98.3 ± 0.2	95.8 ± 0.2	95.7 ± 0.3	92.2 ± 0.3	94.3 ± 0.3	97.2 ± 0.5	95.2 ± 0.6
	[^{89}Zr]Zr-TRITA	85.8 ± 0.9	21.1 ± 0.9	18.4 ± 0.5	76.2 ± 1.0	87.9 ± 0.3	67.7 ± 0.9	70.4 ± 0.9
5 d	**[^{89}Zr]Zr-PCTA**	**100**	**100**	**100**	**100**	**100**	**100**	**100**
	[^{89}Zr]Zr-NOTA	97.4 ± 0.3	94.4 ± 0.5	94.8 ± 0.6	90.2 ± 0.3	91.8 ± 0.6	97.0 ± 0.3	93.4 ± 0.1
	[^{89}Zr]Zr-TRITA	77.8 ± 1.1	16.5 ± 2.7	15.4 ± 0.8	68.1 ± 1.5	85.5 ± 1.1	59.2 ± 0.7	67.6 ± 0.5
7 d	**[^{89}Zr]Zr-PCTA**	**100**	**100**	**100**	**100**	**100**	**100**	**100**
	[^{89}Zr]Zr-NOTA	96.2 ± 0.2	90.4 ± 0.4	92.9 ± 0.7	87.8 ± 0.9	90.6 ± 0.4	96.3 ± 0.4	89.5 ± 1.5
	[^{89}Zr]Zr-TRITA	70.4 ± 0.8	9.4 ± 0.7	7.3 ± 0.6	59.7 ± 0.5	83.9 ± 0.5	57.2 ± 0.6	61.8 ± 1.2

Table 4.

Chronological *in vitro* serum stability study of [^{89}Zr]Zr-complexes in human serum maintained at 37°C for 7 days as determined by size exclusion chromatography (n = 3 for each [^{89}Zr]Zr-complex at each time point)

Time point	% Intact of [^{89}Zr]Zr-complexes (n = 3)		
	[^{89}Zr]Zr-PCTA	[^{89}Zr]Zr-NOTA	[^{89}Zr]Zr-TRITA
0 h	100	100	100
1 d	99.9 ± 0.1	97.7 ± 0.2	80.8 ± 1.1
3 d	99.8 ± 0.1	95.5 ± 0.4	59.1 ± 1.5
5 d	99.6 ± 0.2	91.8 ± 0.3	45.2 ± 2.4
7 d	99.4 ± 0.2	89.2 ± 0.5	32.4 ± 0.6

Table 5.

Dosimetry comparison of [^{89}Zr]Zr-PCTA, [^{89}Zr]Zr-TRITA and [^{89}Zr]Zr-NOTA

Tissue/Organ	Dose per Administered Activity (mGy/MBq)				
	[^{89}Zr]Zr-DFO	[^{89}Zr]Zr-DOTA	[^{89}Zr]Zr-NOTA	[^{89}Zr]Zr-PCTA	[^{89}Zr]Zr-TRITA
Brain	2.0	1.8	2.2	2.1	54.6
Large Intestine	3.1	21.0	17.1	8.5	28.8
Small Intestine	2.0	5.0	4.7	2.8	16.8
Stomach Wall	15.6	19.1	10.7	41.1	55.6
Heart	2.1	2.0	2.4	2.2	53.3
Kidneys	2.0	2.7	2.7	2.1	16.2
Liver	2.1	2.2	2.4	2.3	33.4
Lung	3.1	2.3	3.0	3.4	151.0
Pancreas	4.3	3.3	3.2	2.7	16.6
Skeleton	8.5	4.2	6.9	10.2	679.0
Spleen	8.4	3.0	3.3	3.3	17.9
Testes	2.0	2.2	2.4	2.0	13.9
Thyroid	2.4	2.1	2.6	2.5	76.0
Urinary Bladder	29.9	30.3	30.4	30.0	41.6
Total Body	2.3	2.4	2.7	2.5	65.0